

A conceptual model for glacial lake bathymetric distribution

Taigang Zhang^{1,2,3}, Weicai Wang² Wang¹, Baosheng An² An^{1,4}

¹State Key Laboratory of Tibetan Plateau Earth System, Environment and Resources (TPESER), Institute of Tibetan Plateau Research, Chinese Academy of Sciences, Beijing 100101, China

²College of Earth and Environmental Sciences, Lanzhou University, Lanzhou 730000, China

³State Key Laboratory of Tibetan Plateau Earth System, Environment and Resources (TPESER), Institute of Tibetan Plateau Research, Chinese Academy of Sciences, Beijing 100101, China

³Center for the Pan-Third Pole Environment, Lanzhou University, Lanzhou 730000, China

⁶~~School~~⁴School of Science, Tibet University, Lhasa 850011, China

Correspondence: Taigang Zhang (zhangtg16@lzu.edu.cn) and Weicai Wang (weicaiwang@itpcas.ac.cn)

Abstract. The formation and expansion of glacial lakes worldwide due to global warming and glacier retreat have been well documented in the past few decades. Thousands of glacial lake outburst floods (GLOFs) originating from moraine-dammed and ice-dammed lakes were reported, causing devastating impacts on downstream lives and properties. Detailed glacial lake bathymetry surveys are essential for accurate GLOF simulation and risk assessment. However, these bathymetry surveys are still scarce as glacial lakes located in remote and high-altitude environments hamper a comprehensive investigation. We developed a conceptual model for glacial lake bathymetric distribution using a semi-automatic simulation procedure. The basic idea is that the statistical glacial lake volume-area curves conform to a power-law relationship indicating that the idealized geometric shape of the glacial lake basin should be hemispheres or cones. First, by reviewing the evolution of various types of glacial lakes, we identified ~~10~~⁹ standard conceptual models to describe the shape of lake basins. Second, we defined a general conceptual model to depict the continuum transitions between different standard conceptual models for those specific glacial lakes that lie between two standard conceptual models. Third, we nested the optimal conceptual model into the actual glacial lake basin to construct the water depth contours and interpolate the glacial lake bathymetric distribution. We applied the conceptual model to simulate ~~three-six~~ typical glacial lakes in the ~~Tibetan Plateau~~High Mountain AsiaThird Pole with in-situ bathymetric surveys to verify the algorithm's applicability. The results show a high consistency in the point-to-point comparisons of the measured and simulated water depths with a total volume difference of approximately $\pm 10\%$. The

29 conceptual model has significant implications for understanding glacial lake evolution and modeling GLOFs in the
30 future.

31

32 **1 Introduction**

33 Globally, glacial recession and thinning have been well-documented over the last decades via field observations
34 and remote sensing techniques (Yao et al., 2012; Zemp et al., 2019; Hugonnet et al., 2021). Such evolution of glaciers
35 due to climate warming and anthropogenic factors could induce related effects (Yao et al., 2019), among which is the
36 expansion and formation of glacial lakes (Zhang et al., 2015; Emmer et al., 2016; Wang et al., 2020; Ma et al., 2021).
37 Glacial lakes are water bodies developed within depressions of glacier moraine or mainly fed by contemporary glacier
38 meltwater (Yao et al., 2018). Due to glacier retreats, they are generally impounded by glacier terminal or lateral
39 moraine. Since the 1990s, the glacial lakes [within 1 km buffer of the contemporary glaciers](#) worldwide have increased
40 by around 50% in total number, area, and volume (Shugar et al., 2020), ~~manifesting an ongoing climate change~~.
41 These changes have also been accompanied by glacial lake outburst flood (GLOF) risks.

42 As a glacier-related hazard, GLOF has been a frequent incidence in various glacierized areas, causing
43 considerable socioeconomic losses (Anaconda et al., 2015a; Nie et al., 2018; [Emmer et al., 2022a](#)). According to a
44 compilation ~~by Carrivick and Tweed (2016)~~, [more than approximately 1000-3,000](#) GLOFs from moraine- and ice-
45 dammed lakes are recorded worldwide and claim more than 10,000 deaths ([Carrivick and Tweed, 2016; Lützow et](#)
46 [al., 2023](#)). Under the triggering factors such as ice avalanches, landslides, and heavy precipitation, glacial lakes are
47 extremely unstable and subsequently cause a sudden release of water with peak discharge higher than a dozen times
48 that of monsoon rainfall floods (Richardson and Reynolds, 2000; Westoby et al., 2014; Kougkoulos et al., 2018).
49 However, due to the relatively small volume of the glacial lake, the flooding process generally ~~attenuate~~[proceeds](#)
50 rapidly within a few hours. Knowledge of glacial lake volume is critical, as it influences the released water volume
51 and GLOFs magnitude (Fujita et al., 2013). Therefore, lake volume is often employed as an essential criterion in
52 numerous cases of GLOF susceptibility and risk assessment (Bolch et al., 2011; Aggarwal et al., 2017; Drenkhan et
53 al., 2019; Falatkova et al., 2019).

54 Currently, only sporadic bathymetric surveys on glacial lakes have been conducted worldwide. In Cordillera
55 Blanca, Peru, facing continuous threats by GLOFs (Lliboutry et al., 1977), more than 100 detailed bathymetric
56 surveys of glacial lakes have been carried out to [better](#) understand ~~better~~ the regional GLOF risks (Muñoz et al.,

2020). Government agencies and research institutions have promoted these surveys. In the [Tibetan Plateau and its surroundings](#)[High Mountain Asia](#)[Third Pole region](#), the bathymetric surveys are focused on the glacial lakes in the Himalayas (Sharma et al., 2018; Watson et al., 2018), where approximately 60 bathymetric surveys of glacial lakes, such as the Cirenmaco, Jialongco, and Longbasaba Lake, were conducted (Yao et al., 2012; Wang et al., 2018; Li et al., 2021). They measure the water depth with ultrasonic devices onboard automatic uncrewed boats or manual hovercrafts.

Performing a universal investigation campaign of lake bathymetry is impractical for thousands of glacial lakes in remote areas and high elevations. Instead, scholars typically utilize single total lake volume data rather than bathymetric distribution in GLOF modeling (Anaconda et al., 2015b; Zhang et al., 2021). The lake volume is typically estimated by empirical equation, e.g., direct volume–area equation (O'Connor et al., 2001; Huggel et al., 2002; Loriaux and Casassa, 2013), or indirect area–mean depth/maximum depth/width equation (Wang et al., 2012), which have considerable uncertainty. There is no doubt that the measured and/or interpolated glacial lake bathymetric distribution have great merit that can precisely determine the maximum potential outburst volume of the glacial lake, serving to further simulate the GLOF propagation and evaluate downstream exposures (Frey et al., 2018; Sattar et al., 2021). Moreover, a bathymetry survey is also pivotal to understanding the interactions between the glaciers and their terminating lakes ([Zhang et al., 2023](#)), as several studies have revealed that the proglacial lake bathymetric state can dominate the glacier terminal melting and calving regimes ([Watson et al., 2020](#); Sugiyama et al., 2021).

Can we obtain glacial lake bathymetric distributions through modeling rather than in situ investigations? Previous studies have provided insights. Cook and Quincey (2015) preliminarily proposed that the same type of glacial lakes may have their idealized geometric shapes, which depict the evolution of glacial lakes' volume–area (V–A) relationship over time. For instance, the triangular cone is suitable to represent the idealized geometric shape of ice-dammed lakes dammed by glaciers and formed in the narrow valley. The idealized conceptual models of glacial lakes can be combined with the actual situations to project the glacial lake bathymetric distribution.

An idealized lake basin is also helpful in constructing numerical or physical models. In the study of Veh et al. (2020), the conceptual model of glacial lakes was constructed as a semi-ellipsoid with a circular surface to calculate the released volume after the lake drainage. The surface area and height of the semi-ellipsoid refer to the glacier lake area and maximum water depth, respectively. Based on these instructive designs, we attempted to develop a procedure and algorithm for modeling glacial lake bathymetric distribution in this study. We first (i) retrieved as many as

85 possible conceptual models for various types of glacial lakes by reviewing the evolutions of glacial lakes and
86 analyzing the relationships between lake volumes and areas; (ii) explored the procedure and algorithm to estimate
87 bathymetric distribution in conjunction with actual lake surface and basin shapes; and then (iii) discussed their
88 implications and potential applications.

89 **2 Data and methods**

90 **2.1 Compilation of glacial lake bathymetry**

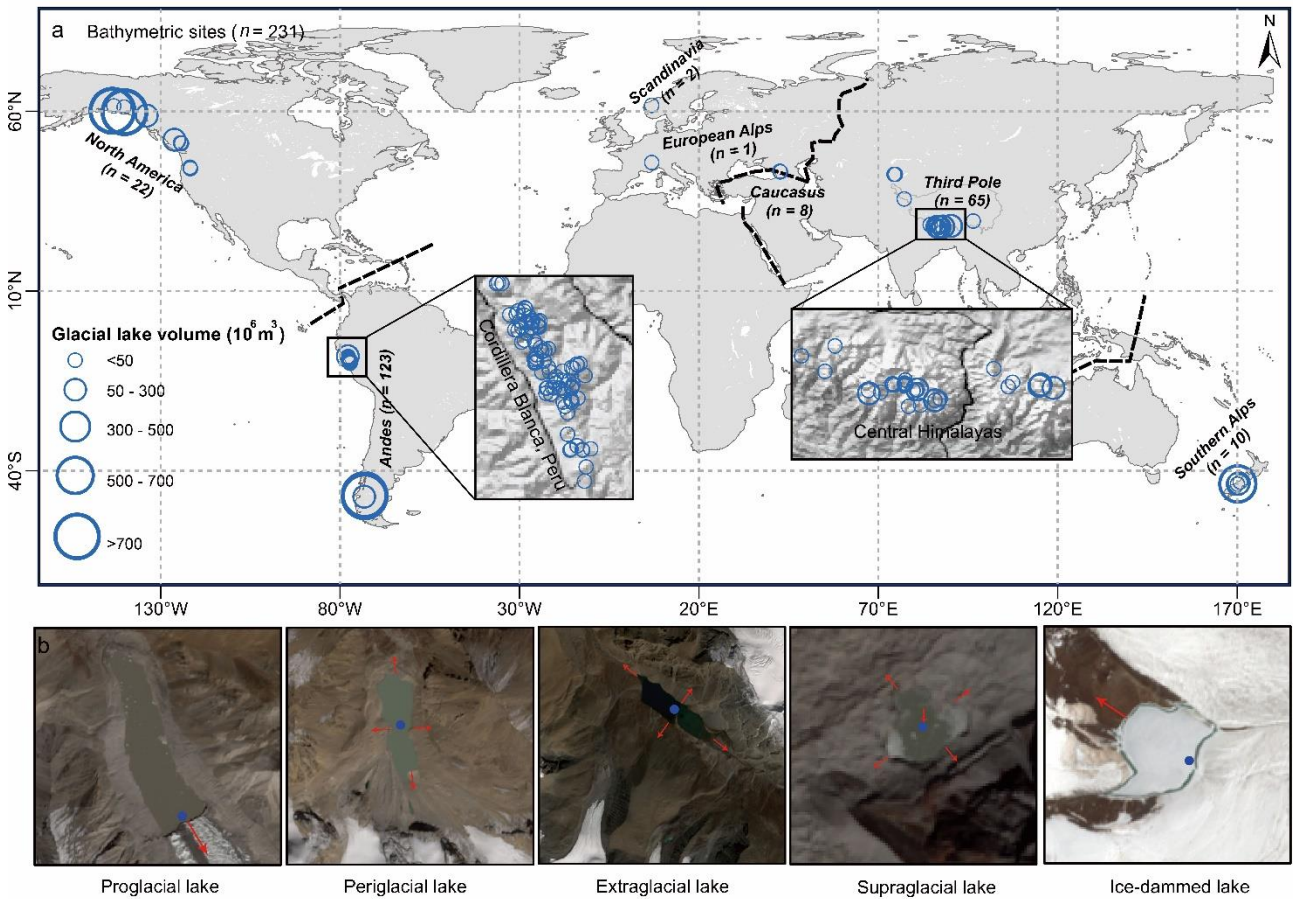
91 Analyzing the existing glacial lake bathymetries can help us reveal glacial lake water depth characteristics. To
92 our knowledge, more than 60 articles have mentioned surveyed bathymetry data from glacial lakes. We integrated
93 the prior studies and established an inventory of global glacial lake bathymetry (Supplementary material 1). The
94 attributes included the name, location, survey time, area, volume, and maximum water depth. A total of 231
95 bathymetric data from 220 glacial lakes globally were compiled in the inventory (Fig. 1a). Some large glacial lakes
96 were eliminated since their area left deviate from the majority of concentration zone posing the dispersion of our data
97 and which could reduce the fitting accuracy (Cook and Quincey, 2015).

98 **2.2 Classification and evolution of different glacial lake types**

99 The maximum water depth (D) and total volume (V) are the fundamental parameters regarding the idealized
100 geometric shape of glacial lakes. We used the compiled glacial lake bathymetry data to fit the curves of V–A (glacial
101 lake area) and D–A to understand the evolution-potential shapes of an idealized lake basing glacial lakes and to develop
102 a conceptual model suitable for describing the shape of an idealized lake basin. Based on the topological positions
103 between the glacial lakes and their parent glaciers, we classified glacial lakes as proglacial, periglacial, extraglacial,
104 supraglacial, ~~proglacial, periglacial, extraglacial,~~ and ice-dammed types (Fig. 1b). This classification system
105 considers glaciers' critical role in the evolution of glacial lakes (Petrov et al., 2017; Rick et al., 2022).

106 We assumed that different types of glacial lakes have different expansion mechanisms and, thus, different
107 conceptual models. The proglacial lake's expansion mainly proceeds backward by glacial retreat. The periglacial lake
108 and the extraglacial lake are not directly in contact with the glacier, and their expansion depends more on changes in
109 precipitation and glacier meltwater, thereby potentially expanding in all horizontal directions. As for the supraglacial
110 lakes, expansion proceedss in all directions, and the temperature difference at the ice-water interface continuously
111 melts the glacier ice in both horizontal and vertical orientations. While for ice-dammed lake, the evolution often

112 appears horizontally with glacier retreat. The periglacial lake and the extraglacial lake are not directly in contact with
 113 the glacier, and their expansion depends more on changes in precipitation and glacier meltwater, thereby potentially
 114 expanding in all horizontal directions. ~~The proglacial lake's expansion mainly proceeds backward by glacial retreat.~~
 115 These various mechanisms in glacial lake expansions showed that the changes in the lake basin among the different
 116 glacial lake types are inconsistent, indicating that they may have different conceptual models.



117
 118 **Figure 1.** (a) Distribution of glacial lakes whose volume was surveyed in detail. (b) Glacial lakes were divided into five categories,
 119 namely proglacial (direct in contact with glacier terminus), periglacial (separated from the glacier and dammed by historical moraine),
 120 extraglacial (far from the glacier and generally dammed by landslides), supraglacial (positioned on the glacier surface), ~~proglacial (direct~~
 121 ~~in contact with glacier terminus), periglacial (separated from the glacier and dammed by historical moraine), extraglacial (far from the~~
 122 ~~glacier and generally dammed by landslides), supraglacial (positioned on the glacier surface), and ice-dammed lake (formed when glacier~~
 123 ~~surges block downstream valleys or meltwater fills depressions between retreating tributary and main glaciers).~~ Red arrows indicate the
 124 possible main directions of expansion of the glacial lake, and the blue points represent the location of maximum water depth.

126 2.3 Standard conceptual model

127 The basic procedure of constructing glacial lake bathymetric distribution is to (i) identify the most appropriate
128 conceptual model that can describe the idealized lake basin, (ii) calculate the theoretical formulation equations of this
129 conceptual model, (iii) nest this conceptual model into the actual glacial lake basin to construct the water depth
130 contours, and (iv) interpolate and calculate the glacial lake bathymetric distribution. The conceptual model was
131 constructed as the scheme presented by Veh et al. (2020). Glacial lakes were assumed to have hemispherical or similar
132 three-dimensional lake basin shapes. The standard surface of the glacial lake was assumed to be an ellipse.

133 The general formula between the volume and area of glacial lakes fits a power-law relationship (Table 1). It
134 could be expressed as Eq. (1). The best-fit curve for the relationship between maximum water depth and area of
135 glacial lakes also follows the power-law relationship (Eq. 2) (Fig. 2).

$$136 \quad V = \alpha A^\beta \quad (1)$$

$$137 \quad D = \gamma A^\varepsilon \quad (2)$$

138 A is the area of the glacial lake; α , β , γ , and ε are the coefficients. The value of β is greater than 1, and
139 ε is less than 1.

140 The three-dimensional bodies representing the standard shape of a lake basin were required to have a general
141 formula as defined by Eq. (3):

$$142 \quad V = \delta AD \quad (3)$$

143 Here, δ is the coefficient, A is the elliptical surface area, and D corresponds to the maximum water depth of
144 the glacial lake. We identified four hemispheres or cones whose volumes can be expressed by Eq. (3): the hemisphere
145 structured by the elliptical side ($V = 2/3AD$); the hemisphere structured by the upward-opening parabolic side ($V =$
146 $1/2AD$); the cone structured by the straight side ($V = 1/3AD$); and the cone structured by the rightward-opening
147 parabolic side ($V = 1/5AD$). These bodies are defined as the standard conceptual model (SCM), and their curves in
148 the X-O-Z quadrant are called the standard curves (Fig. 3a). These four standard curves are progressively concave
149 inward in the quadrant, from the elliptical curve to the rightward-opening parabolic curve.

150 These SCMs for the supraglacial, periglacial, and extraglacial lake ~~types~~ are compatible with the expansion
151 mechanisms partly because their growth direction is comprehensive at the horizontal level. Their maximum water

152 depths were set in the lake center-lake. However, proglacial and ice-dammed lakes are different. Their expansions
153 are focused toward the glacier's or valley's direction, and the maximum water depths are generally situated near the
154 intersection with the glacier. Under these circumstances, we considered the SCMs of proglacial lakes to be half of
155 the preceding four SCMs, such as namely the semi-hemisphere structured by the elliptical side ($V = 1/3AD$); the semi-
156 hemisphere structured by the upward-opening parabolic side ($V = 1/4AD$); semi-cone structured by the straight side
157 ($V = 1/6AD$); and the semi-cone structured by the rightward-opening parabolic side ($V = 1/10AD$). ~~We also took into~~
158 ~~account the way in which the SCMs of the ice-dammed lake formed.~~ We ~~ultimately~~-designed two SCMs for the ice-
159 dammed lake (Fig. 3a): the semi-cone structured by the straight side ($V = 1/6AD$) and the triangular cone ($V = 1/3A-D$).
160 The deepest point for proglacial and ice-dammed lake were set near the glacier-lake interface. Most of the actual
161 volume points lie between the volume curves of these SCMs (Fig. 4), and there are one or two closer SCM volume
162 curves for each type of glacial lake's fitted A–V curve. Ultimately, a total of 9 different SCMs were designed to
163 express the idealized geometric shapes of glacial lake basin.

164

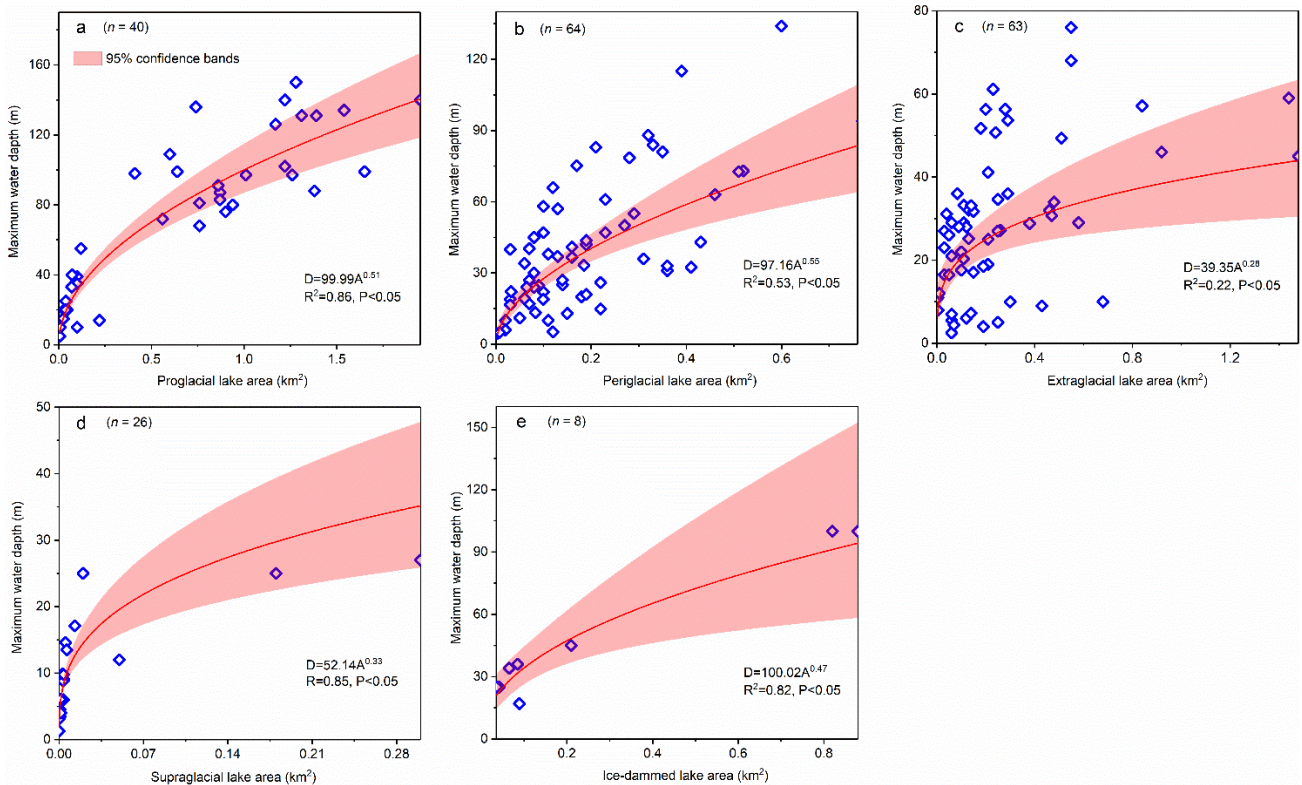
165 **Table 1.** Empirical equations of volume and area of glacial lakes in previous studies. The applicable region, lake type, and sample size
166 for each empirical equation were indicated during fitting. The volume unit is 10^6 m^3 , and the area unit is km^2 . In the dam material-
167 based classification method for glacial lakes, a substantial number of proglacial and periglacial lakes can be categorized as moraine-
168 dammed lakes.

ID	Empirical formulas	Region	Lake types	Samples	Reference
1	$V = 35A^{1.5}$	British Columbia, Canada	Ice-dammed lake	not mentioned	Evans, 1986
2	$V = 168.5A^2 + 3.11A$	Northwestern America	Moraine-dammed lake	7	O'Connor et al., 2001
3	$V = 34.44A^{1.42}$	Worldwide	Moraine- and ice-dammed lake	13	Huggel et al., 2002
4	$V = 43.24A^{1.53}$	Himalayas	Moraine-dammed lake	17	Sakai, 2012
5	$V = 6.07A^{1.37}$	Himalayas	Moraine-dammed lake	20	Wang et al., 2012
6	$V = 55A^{1.25}$	Himalayas	Moraine-dammed lake	20	Fujita et al., 2013
7	$V = 33.58A^{1.39}$	Worldwide	Moraine- and ice-dammed lake	31	Loriaux and Casassa, 2013
8	$V = 42.93A^{1.48}$	Peruvian Andes	Moraine- and bedrock-dammed lake	35	Emmer and Vilímek, 2014
9	$V = 34.07A^{1.37}$	Worldwide	Various types	69	Cook and Quincey, 2015
10	$V = 11.49A^{1.26}$	Worldwide	Supraglacial lake	9	Cook and Quincey, 2015
11	$V = 60A - 6.28$	Worldwide	Moraine-dammed lake	42	Cook and Quincey, 2015
12	$V = 2.63e^A$	Worldwide	Ice-dammed lake	9	Cook and Quincey, 2015
13	$V = 37.3A^{1.47}$	Himalayas	Moraine-dammed lake	33	Khanal et al., 2015
14	$V = 52.2A^{1.18}$	Himalayas	Proglacial lake	6	Sharma et al., 2018
15	$V = 40A^2 + 5.06A$	Himalayas	Moraine-dammed lake	17	Patel et al., 2017
16	$V = 35.36A^{1.47}$	Central Asia	Moraine-dammed lake	32	Kapitsa et al., 2017
17	$V = 32.13A^{1.49}$	Himalayas	Ice-dammed lake, supraglacial lake	not mentioned	Miles et al., 2018

18	$V = 28.95A^{1.33}$	Worldwide	Moraine-dammed lake	93	Watson et al., 2018
19	$V = 35.46A^{1.4016}$	Himalayas	Supraglacial lake	24	Watson et al., 2018
19	$V = 41WA + 2A$	Cordillera Blanca, Peru	Moraine-dammed lake	120	Muñoz et al., 2020
20	$V = 37.36A^{1.41}$	Peruvian Andes	Various types	170	Wood et al., 2021
21	$V = 38.04A^{1.36}$	Peruvian Andes	Moraine-dammed lake	not mentioned	Wood et al., 2021
22	$V = 43.27A^{1.64}$	Peruvian Andes	Unclassified	not mentioned	Wood et al., 2021

169

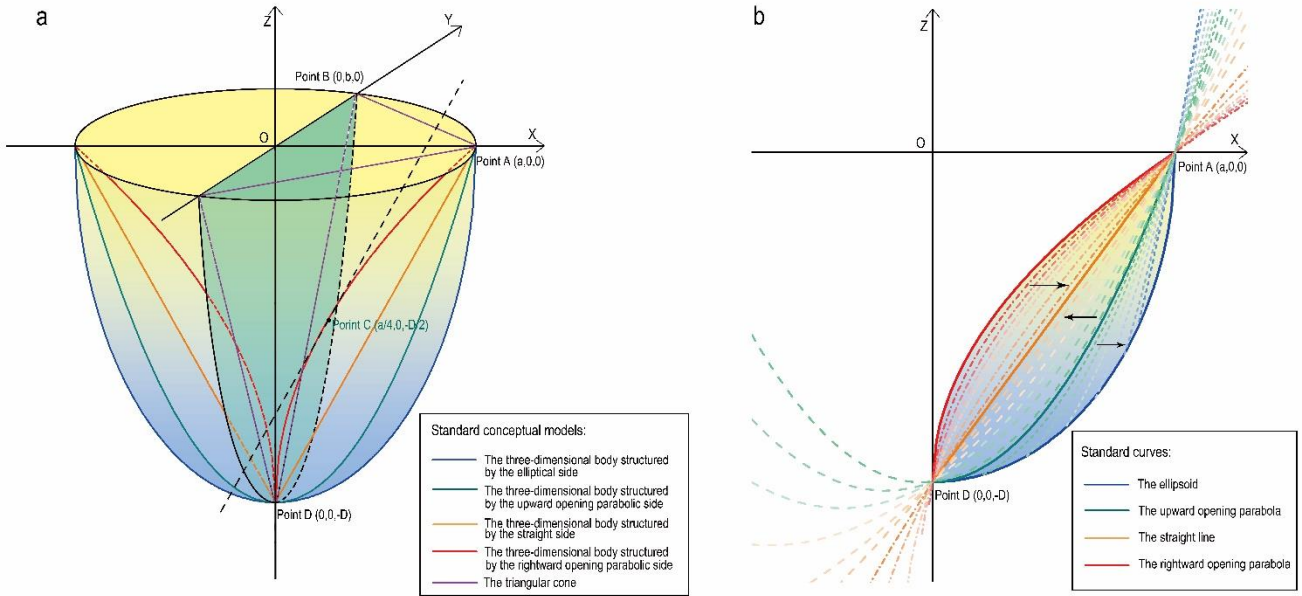
170



171

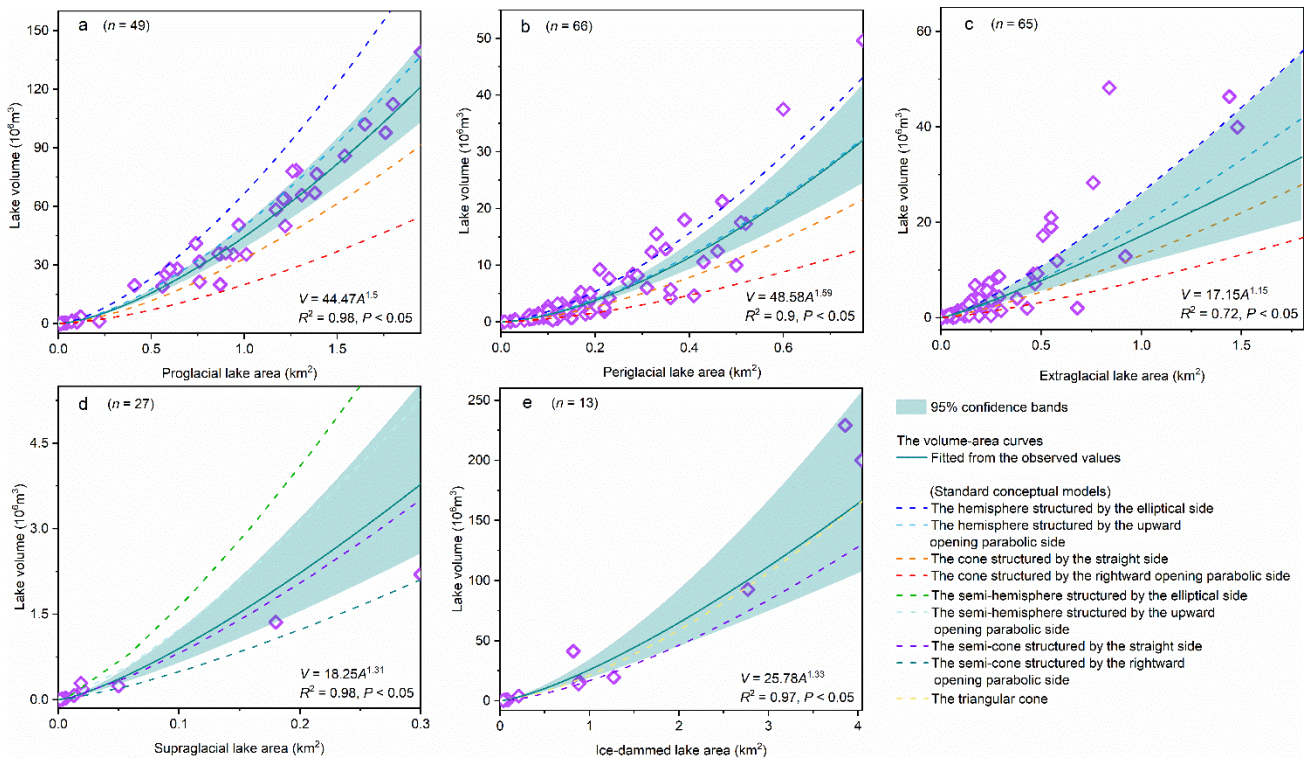
172 **Figure 2.** Relationships between maximum water depth and the area of glacial lakes were compiled in the present study for the following

173 lake types: (a) proglacial lake, (b) periglacial lake, (c) extraglacial lake, (d) supraglacial lake, and (e) ice-dammed lake.



174

175 **Figure 3.** (a) Schematic diagram illustrates the shapes of the SCMs, namely the hemisphere structured by the elliptical side/upward-
 176 opening parabolic side, the cone structured by the straight side/rightward-opening parabolic side, the triangular cone, as well as their
 177 shapes when symmetrically divided matching the SCMs of the proglacial lake. Here, A is the semi-long axis, B is the elliptical surface's
 178 semi-short axis, and D is the maximum water depth. (b) Convergences of the general curves towards the standard curves in the X–O–Z
 179 quadrant in different orientations.



180

181 **Figure 4.** Relationships between the volume (V) and area (A) of glacial lakes were compiled in the present study for the following lake

182 types: (a) proglacial lake, (b) periglacial lake, (c) extraglacial lake, (d) supraglacial lake, and (e) ice-dammed lake. The dotted lines
183 indicate the volume curves of different standard conceptual models, which were fitted by Eq. (2) and (3). ~~The V-A curves of standard~~
184 ~~conceptual models of the proglacial lake type are half the normal condition.~~

185 2.4 General conceptual model

186 ~~The closest SCM likely does not represent the most appropriate conceptual model if~~ If a specific glacial lake
187 ~~has determines determined~~ its parameters such as surface size, ~~type~~ maximum water depth, and volume, it is unlikely
188 that the closest SCM would accurately represent the most appropriate conceptual model. This is because the relatively
189 inherent volume of the SCM is hardly equal to the volume of a specific glacial lake. In other word, ~~t~~ ~~The SCM~~ volume
190 curve of the SCM is is constant, and therefore. ~~However,~~ the volume point of a specific glacial lake ~~does may not~~
191 ~~necessarily coincide with~~ deviate from the SCM volume curve. Consequently, directly ~~Thus, using~~ the SCM
192 ~~directly~~ to nest and interpolate a realistic glacial lake bathymetric distribution would result in an initial over- or
193 underestimation of the total lake volume.

194 The SCMs can only help us comprehend the various glacial lake morphologies; they cannot be applied directly
195 to estimate the glacial lake bathymetric distribution. We may conceive the measured volume points between the SCM
196 volume curves as a result of the transition from one SCM to another. For instance, from the upward-opening parabolic
197 line to the straight line, it is the standard parabolic line continuously approximating the straight line on the X-O-Z
198 quadrant by moving downward and left (Fig. 3b). During the movement process, the rotated-out hemisphere is
199 moving toward the cone structured by the straight side. We can capture these general conceptual models (GCMs) in
200 this transition stage and make their volume consistent with the measured or estimated lake volume. This means we
201 find a GCM that is more effective than the SCM in estimating the lake depth distribution.

202 Python programming was used to drive the standard curves' transition and parameter calculations. The
203 theoretical description for the GCMs is presented in supplementary material 2. By relocating the standard curve's
204 vertices and altering the opening size, it is simple to compute the transition of a standard upward/rightward-opening
205 parabola to a straight line. The resultant general curves must pass through points A and D. The convergence to the
206 standard elliptic curve from the standard upward-opening parabola is relatively complicated. If we move the vertices
207 of the standard parabola to the right and downward, the maximum height of the produced GCM changes. We used a
208 compound style here. When the second intersection of the moved general parabolic curve and the standard elliptic
209 curve occurs (from right to left), the side of GCM starts to take the elliptic curve change. Additionally, the marginal

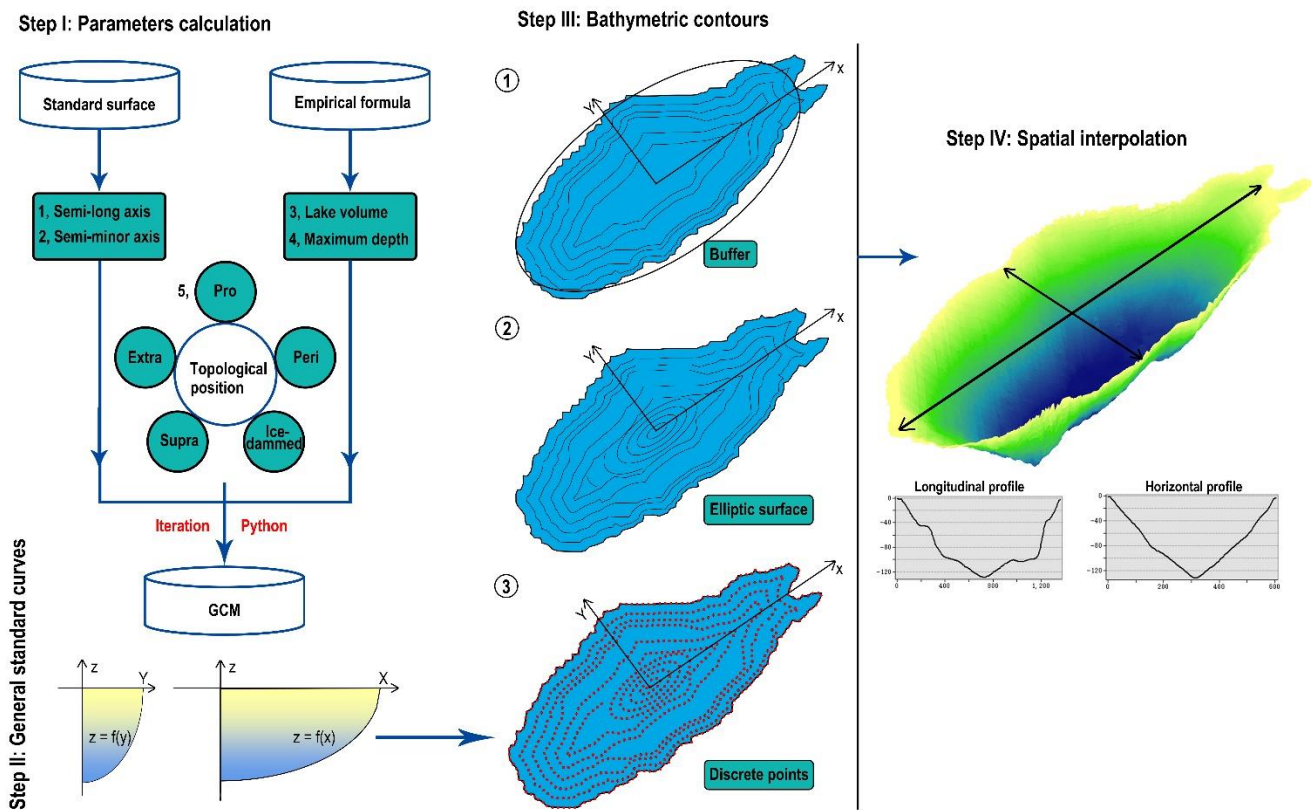
210 SCMs should be employed when the measured volume is larger (smaller) than the largest (smallest) SCM volume.

211 **2.5 Nesting the actual glacial lake shapes**

212 Once a given glacial lake's GCM has been established, the lake's bathymetric contours may be predicted in
213 relation to actual conditions and parameters. Since the actual shape of the glacial lake surface is irregular, rather than
214 the normal elliptic surface we used in the models, it was crucial to [determine](#) how the depth contours move inward
215 based on the actual shape.

216 We tested two hypotheses. First, utilizing the lakeshore line to continually create buffers inward might depict
217 the depth contours because the depth contours near the lakeshore were the consequence of ongoing indentation of the
218 actual glacial lake surface outline inward. Second, at the 1/4 semi-long axis of the standard elliptic surface, the depth
219 contours would become progressively blurred as the inward indentation continues, thus subsequently using the
220 standard elliptic surface to start the inward indentation (Fig. 5). Importantly, these assumptions were supported by
221 observations of hundreds of glacial lake bathymetric distribution cases worldwide. Some similarities exist between
222 the bathymetric contours and the lakeshore shape, suggesting that the area near the lakeshore is possibly impacted by
223 the slopes around the lake and/or other material sources. There are two explanations for this phenomenon: either the
224 glacial lakes were continuously filled with exogenous debris and rocks, or the initial lake water level had risen and
225 flooded part of the original slopes.

226 The 1/4 semi-long axis is the ending position where the glacial lake is not impacted by exogenous materials, as
227 determined by our understanding of those SCMs. Most of the glacial lake SCMs were located closer to the cone,
228 structured by the straight side of the hemisphere and the upward-opening parabolic side. It is inferred that the initial
229 deepening of the glacial lake is not particularly large from the outer line to the center (compared to the semi-ellipsoid),
230 indicating that exogenous materials are likely to have impacted it. This situation is better understood when the lake
231 SCM is a cone structured by the rightward-opening parabolic side. Therefore, we hypothesized an extreme
232 circumstance in which a glacial lake starts to be significantly influenced by the lake's surroundings' topography. In
233 this case, the slope of the standard rightward-opening parabolic curve is smaller than the slope of the standard straight
234 line and closer to the ideal deepening state of the lake basin when it is larger. This equal slope point is located at the
235 1/4 semi-long axis and represents half of the maximum water depth.



236

237

Figure 5. The procedure illustrates the parameter calculation of GCMs and processes of creating buffers inward. The water depths on the axes were calculated using the standard curves corresponding to the X and Y axes.

238

239

2.6 Sites for exhibiting and validating results

240

241

242

243

244

245

246

247

248

249

250

251

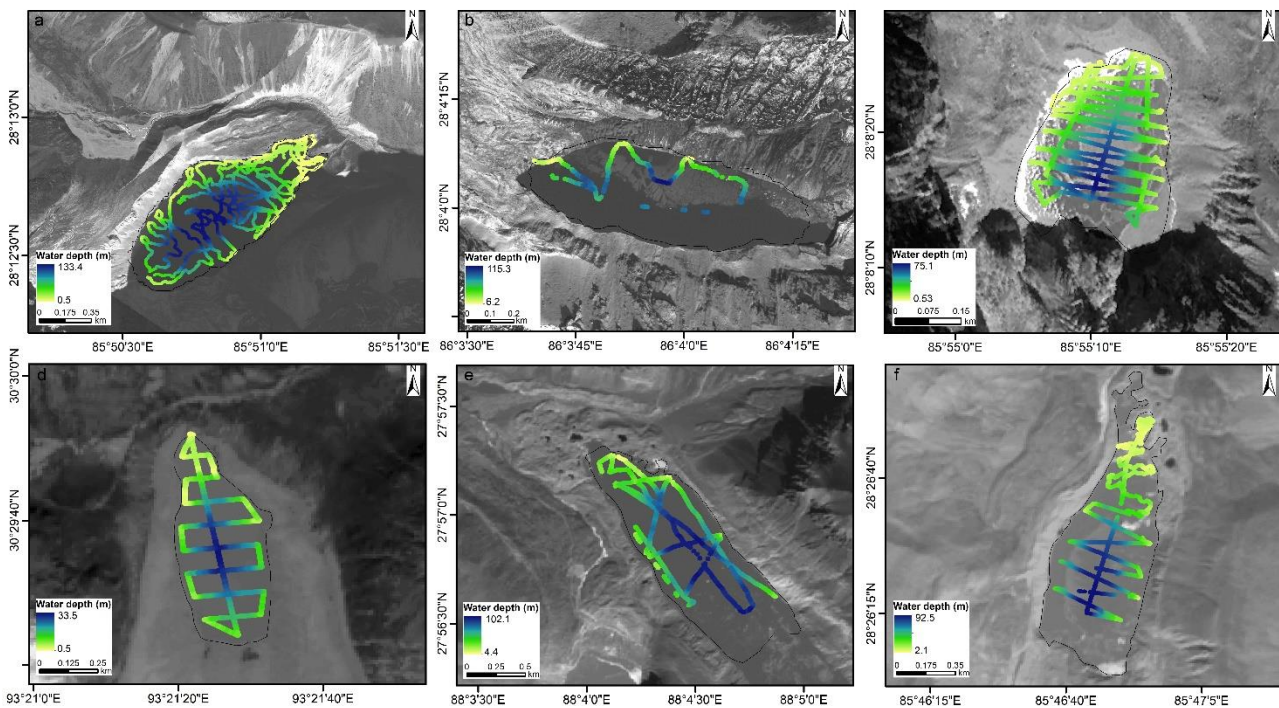
ThreeSix sets of bathymetry data were collected for the typical glacial lakes in the Himalayas and Nyainqentanglha, Tibetan Plateau (Fig. 6). Among them, Jialongco, Cirenmaco and, Jialongco, Poiqu NO.1, and Maqiongco were classified as periglacial lakes, are located in the Poiqu River basin (China-Nepal border). Both lakes experienced GLOFs in 1981 and 2002, causing severe infrastructure losses and transboundary damages (Chen et al., 2013). Th, while the e-Longbasaba Lake and Dasuopuco were classified as proglacial lakes. Although it would be desirable to evaluate the performance of our conceptual models across different types, sizes, and geographic locations of glacial lakes, we were limited by the available observational data and could only conduct these examinations in the High Mountain Asia Third Pole region, focusing on proglacial and periglacial lake types. at the China-India border is a benchmark proglacial lake that has been studied in detail for the glacial lake risks and dynamics of the lake terminating glaciers (Yao et al., 2012; Wei et al., 2021). The topological position, total volume, maximum water depth, and semi-long/minor axis of the standard lake surface were crucial parameters in glacial lake bathymetric distribution modeling (Table 2). The three-six glacial lake bathymetric distributions were simulated

252 according to the lake sizes in the survey year and eventually compared with the measured points of water depths and
 253 the overall parameters (total volume and mean water depth) to verify the feasibility and accuracy of our modeling
 254 method.

255 **Table 2.** The crucial modeling parameters of the ~~three~~ six selected glacial lakes.

Name	Lat°	Lon°	Region	Topological position	Survey year	Area (km ²)	Volume (10 ⁶ m ³)	<u>Mean water depth (m)</u>	Maximum water depth (m)	Semi-long axis (m)	Semi-minor axis (m)
Jialongco	<u>28.21</u>	<u>85.85</u>	<u>Central Himalaya</u>	<u>periglacial</u>	2020	<u>0.61</u>	37.5	<u>58.2</u>	<u>133</u> 133	<u>757</u> 757	<u>314</u> 314
Cirenmaco	<u>28.07</u>	<u>86.07</u>	<u>Central Himalaya</u>	<u>periglacial</u>	2012	<u>0.33</u>	18.0	<u>55</u>	<u>115</u> 115	<u>549</u> 549	<u>185</u> 185
<u>Poiqu NO.1</u>	<u>28.14</u>	<u>85.92</u>	<u>Central Himalaya</u>	<u>periglacial</u>	2021	<u>0.11</u>	<u>2.7</u>	<u>25.5</u>	<u>75.1</u>	<u>242</u>	<u>129</u>
<u>Maqiongco</u>	<u>30.49</u>	<u>93.36</u>	<u>Nyainqentanglha</u>	<u>periglacial</u>	2021	<u>0.23</u>	<u>3.2</u>	<u>15</u>	<u>33.5</u>	<u>493</u>	<u>168</u>
Longbasaba Lake	<u>27.95</u>	<u>88.08</u>	<u>Eastern Himalaya</u>	<u>proglacial</u>	2009	<u>1.17</u>	64.0	<u>48</u>	<u>102</u> 102	<u>1949</u> 194 9	<u>319</u> 319
<u>Dasuopuco</u>	<u>28.44</u>	<u>85.78</u>	<u>Central Himalaya</u>	<u>proglacial</u>	<u>2021</u>	<u>0.55</u>	<u>0.55</u>	<u>33.8</u>	<u>93</u>	<u>1362</u>	<u>247</u>

256



257 **Figure 6.** ~~Locations of~~ The water depth observed along the bathymetric routes for (a) Jialongco, (b) Cirenmaco, (c) Poiqu NO.1, (d)
 258 Maqiongco, (e) Jialongco, and Longbasaba Lake, and (b, e, d)(f) Dasuopuco indications for their water depths along the bathymetric
 259 routes.
 260

261

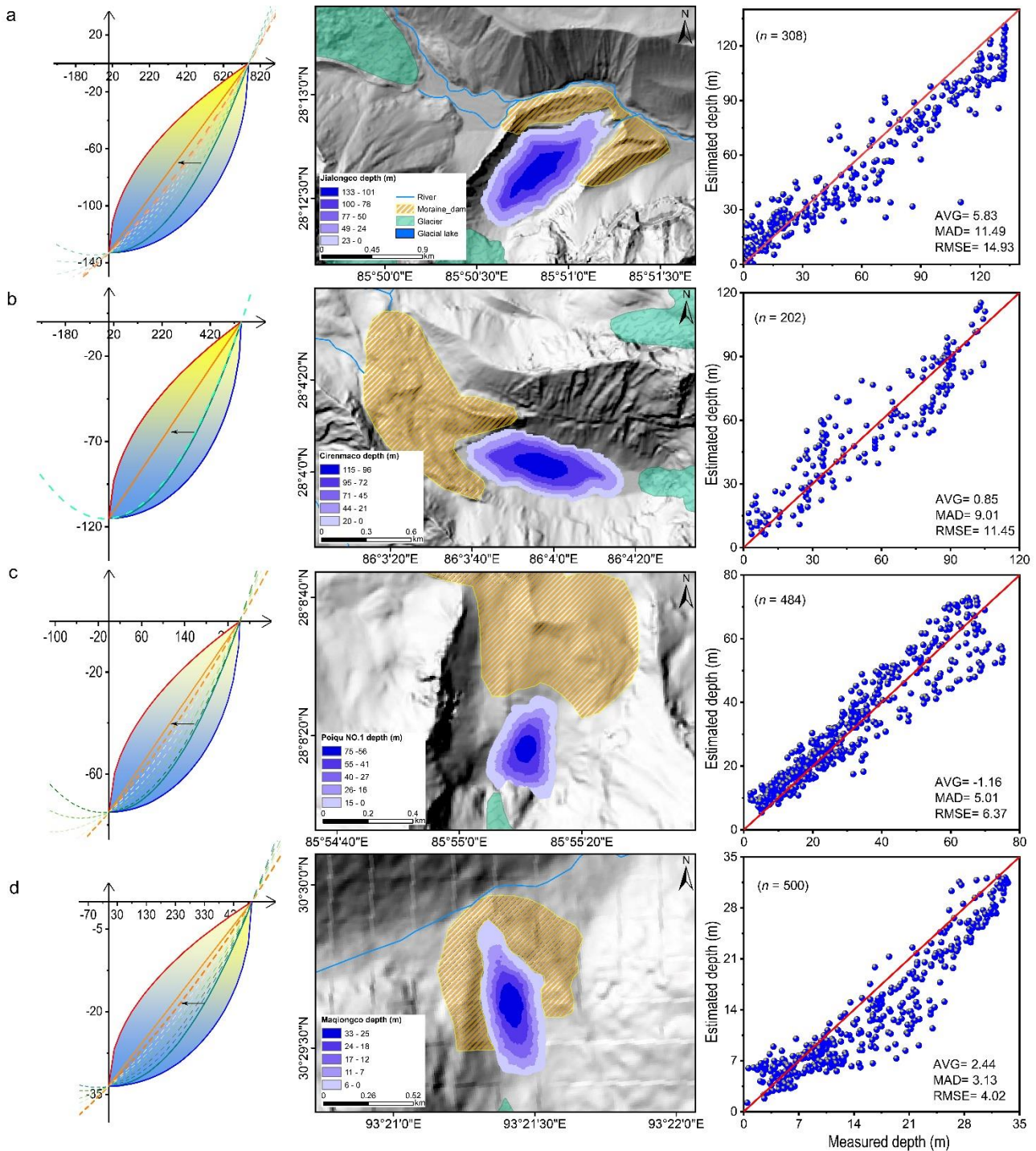
262 3 Results

263 We present the SCMs for each type of glacial lake and demonstrate a procedure to identify the most compatible
264 GCM for a specific glacial lake by equalizing the volume of both. To our knowledge, this is the only (or first) first
265 model to simulate the bathymetric distribution of glacial lakes at present. The results indicate-reveal that the
266 proglacial and periglacial lakes are-exhibit greater depths relatively deep because-as their SCMs are closer to the
267 hemisphere structured by the upward-opening parabolic side. Conversely, The-the SCMs of the extraglacial and
268 supraglacial lakes are closer to the cone structured by the straight side, indicating relatively shallower depths. As the
269 ice-dammed lake, their V-A fitting curve is more similar to the V-A curve of the triangular cone (Fig. 34). Hence,
270 we recommend that the bathymetric distribution modeling for ice-dammed lakes proceeds directly using the standard
271 triangular cone and is not further explored in this study.

272 We determined the optimal GCMs for the three-six exhibited glacial lakes. Following bathymetric distribution
273 modeling results, the total volume of Jialongco was calculated to be $33.1 \times 10^6 \text{ m}^3$ (with a relative error of -11.7%)
274 with a mean water depth of 54.6 m (-8.1%). Its GCM was closer to the cone structured by the straight side (Fig. 7a).
275 The computed Cirenmao total volume and mean depth of Cirenmaco were $17.2 \times 10^6 \text{ m}^3$ (-4.4%) and 51.7 m (-6.9%),
276 respectively. The Cirenmaco GCM had similarities with the hemisphere structured by the upward-opening parabolic
277 side (Fig. 7b), meaning a more significant inward deepening rate than Jialongco. The relatively small-sized Poiqu
278 NO.1 and Maqiongco had total volumes of $2.9 \times 10^6 \text{ m}^3$ (7.4%) and $3 \times 10^6 \text{ m}^3$ (-6.3%), and mean water depths of 27.3
279 m (7.1%) and 12.8 m (-14.7%), respectively. Their optimal GCMs showed similarities with Jialongco (Fig. 7c, d).
280 The proglacial lake, Longbasaba, was estimated to have a total volume of $71.4 \times 10^6 \text{ m}^3$ (11.5%) and a mean depth of
281 61.1 m (22.2%). Its GCM was more resemblant to the semi-ellipsoid (Fig. 7e8a). Dasuopuco had the smallest relative
282 error in the total volume (0.2%) and mean water depth (-1.8%) (Fig. 8b). Overall, aApproximately $\pm 10\%$ volume loss
283 or increase uncertainty was estimated in the process of nesting the general conceptual models to the actual glacial lake
284 shapes.

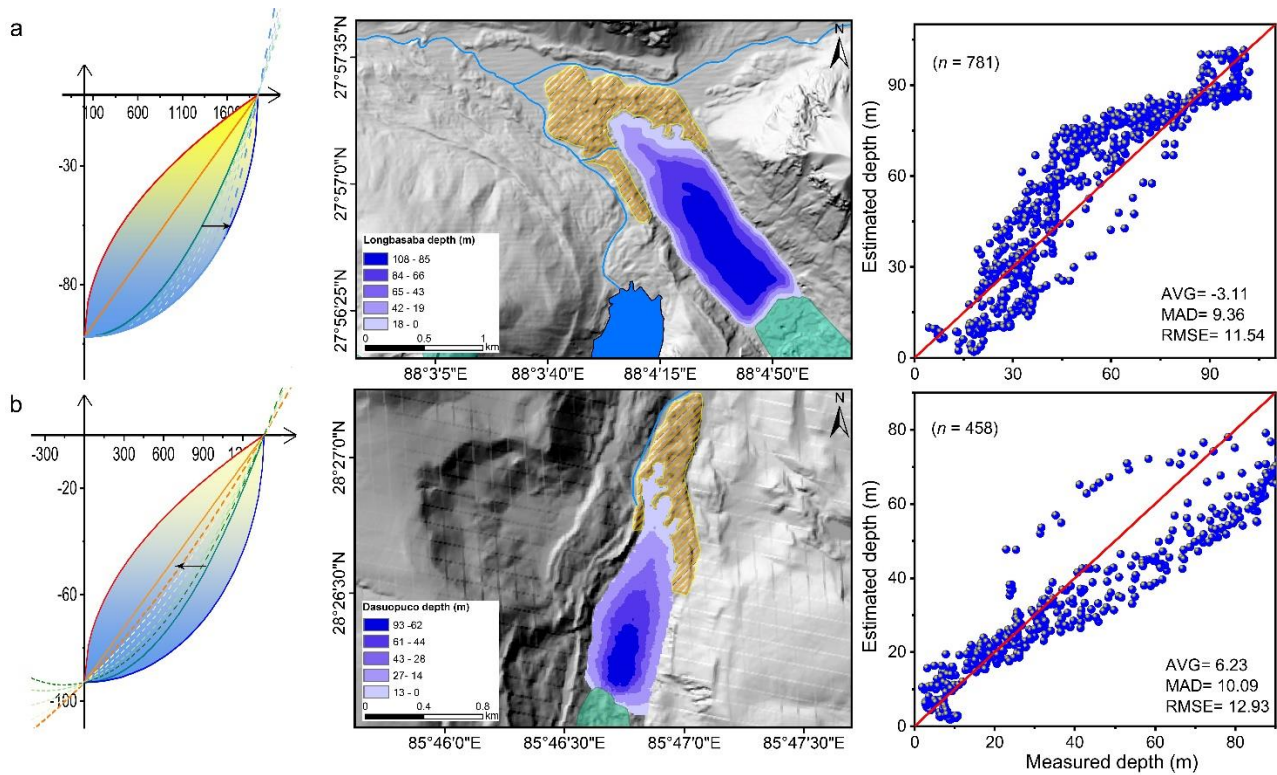
285 The disparity between the area of the assumed standard ellipse surface and the actual lake surface, as well as the
286 deviation of the deepest water location, likely caused the majority of the inaccuracy. The initial settings of glacial
287 lake conceptual models and the algorithm's applicability were confirmed by comparison with the measured and
288 estimated individual water depths. Between the estimated and measured water depths along the bathymetric routes,
289 the average deviation, mean absolute deviation, and root mean root-square error for the three-six glacial lakes all

290 described good consistency. Neither near the lakeshore nor the lake center do the estimates show intolerable
 291 dispersions.



292
 293 **Figure 7.** Modeled glacial lake bathymetric distributions of the four selected periglacial lakes. (a) Jialongco, (b) Cirenmaco, (c) Poiqu
 294 NO.1, and (d) Maqiongco. The average deviation (AVG), mean absolute deviation (MAD), and root mean square error ([EMSERMSE](#))
 295 were selected to depict the consistency between the simulated and measured individual water depths along the boat routes. The

296 movements of the general curves from one standard curve to another are also indicated.



297

298 **Figure 8.** Modeled glacial lake bathymetric distributions of the two selected proglacial lakes. (a) Longbasaba Lake, and (b) Dasuopuco.
299 The average deviation (AVG), mean absolute deviation (MAD), and root mean square error (RMSE) were selected to depict the
300 consistency between the simulated and measured individual water depths along the boat routes. The movements of the general curves
301 from one standard curve to another are also indicated.

302

303 4 Discussion

304 4.1 Glacial lake basin evolution

305 Understanding the glacial lake evolution can help comprehend these idealized geometric shapes in theory. Most
306 moraine- or bedrock-dammed lakes develop in depressions exposed by diminishing glaciers. The supraglacial lakes
307 exist at the glacier snout, eventually facilitating the formation of proglacial and periglacial lakes (Carrivick and Tweed,
308 2013). As the six glacial lakes illustrated, our hypotheses explained the different rates of inward deepening owing to
309 the influence of exogenous materials. The glacier bedrock has been eroded and nudged during historical ice flowing,
310 posing the excavation and growth of glacial lake basins.

311 Contemporary glaciers often have a certain thickness of debris at the snout. For example, approximately 1 m of
312 debris was observed at the snout of the Urumqi Glacier No. 1, China (Echelmeyer et al., 1987) as the result of glacial
313 erosion. The specific sites of continual eroding and nudging spawn overdeepenings and are considered potential
314 glacial lakes (Linsbauer et al., 2016). Since the glacier velocity in the middle part is often larger than that of both
315 sides, the erosion is stronger in the central line of the initial overdeepening. As glacier flowing continues, the shape
316 of the overdeepening finally reaches equilibrium and is similar to a hemisphere, which is the GCM of the lake basin
317 we assumed. After the overdeepenings are exposed, they can be filled by meltwater to form glacial lakes while also
318 receiving material deposition, resulting in a gradual transition of the idealized geometric basin from a hemisphere to
319 a cone. This conjecture can be inferred from the studies of overdeepenings on glacial beds, whereby the volume and
320 surface area of these potential glacial lakes are also in accordance with the power-law relationship (Zhang et al.,
321 2022).

322 4.2 Applicability of the conceptual model

323 Our modeling theory is based on the observations of glacial lake bathymetric distribution characteristics
324 ~~worldwide. The fitted curves of glacial lake volume-area/maximum water depth were derived from the compiled~~
325 ~~inventory of 231 bathymetric data globally, revealing a universal geometrical approximation law for glacial lake~~
326 ~~bathymetry. Therefore and thus,~~ this modeling approach ~~is~~ may be applicable to most glacial lakes in mountain
327 glaciers. ~~However, it is strictly limited by several constraints. Firstly, The~~ the designed conceptual model is more
328 suitable for those glacial lakes with typically lengthy and elliptical-like shapes, ~~and. They~~ may be less applicable ~~for~~
329 ~~very to very~~ irregularly shaped glacial lakes, such as the ice-marginal ~~lakes and thermokarst lakes~~ in the Greenland
330 and Alaska region (Field et al., 2021; Coulombe et al., 2022). Similarly, we ~~had~~ did not collected any glacial lake
331 bathymetry data in polar regions which causes non-applicability on supraglacial lakes over the Greenland/Antarctic
332 Ice sheets. ~~Secondly, the parent glaciers of glacial lakes can be a cirque-valley glacier or a small/medium sized valley~~
333 ~~glacier flowing along a straight valley, ensuring idealized formation conditions for the glacial lake basin with minimal~~
334 ~~erosion and deposition from tributaries.~~

335 Although the simulated results were only validated in the periglacial and proglacial lakes of the Himalayan
336 Himalayas and Nyainqentanglha region due to ~~the~~ limitations of observation data, the comparison results of the
337 measured and modeled depth values at different locations of the ~~three-six~~ glacial lakes ~~reflect~~ demonstrates the
338 rationality and reliability of our conceptual models. ~~To our knowledge, roughly 80% of glacial lakes in the Tibetan~~

339 ~~Plateau and its surroundings can be modeled using this method.~~

340 In addition to the subjective and objective errors made during the modeling phase, there are several systematic
341 defects in the algorithm itself: ~~First, (1) the~~ ~~the~~ total volume and maximum water depth are calculated using
342 empirical equations, which may lead to significant deviations when modeling the bathymetric distribution of an
343 arbitrarily selected glacial lake. ~~In p~~Particularly, the curves of D–A are not robust, with many discrete points
344 appearing (Fig. 2). ~~This affects the modeling results. Therefore, rather than employing the curves based on global~~
345 ~~bathymetry statistics, fitting and using more accurate regionally empirical formulae to reveal local glacial lake~~
346 ~~features is encouraged.~~

347 ~~Second (2); the~~ ~~the~~ estimated depth contours converge inward using the lake shoreline buffers first, followed
348 by the elliptical surfaces. This process may effectively simulate the connections between a bathymetric distribution
349 and glacial lake morphology. However, it is not essential. If the elliptical indentations are always inward relative to
350 the elliptical surface, the modeling accuracy is also not affected significantly in theory: ~~–~~

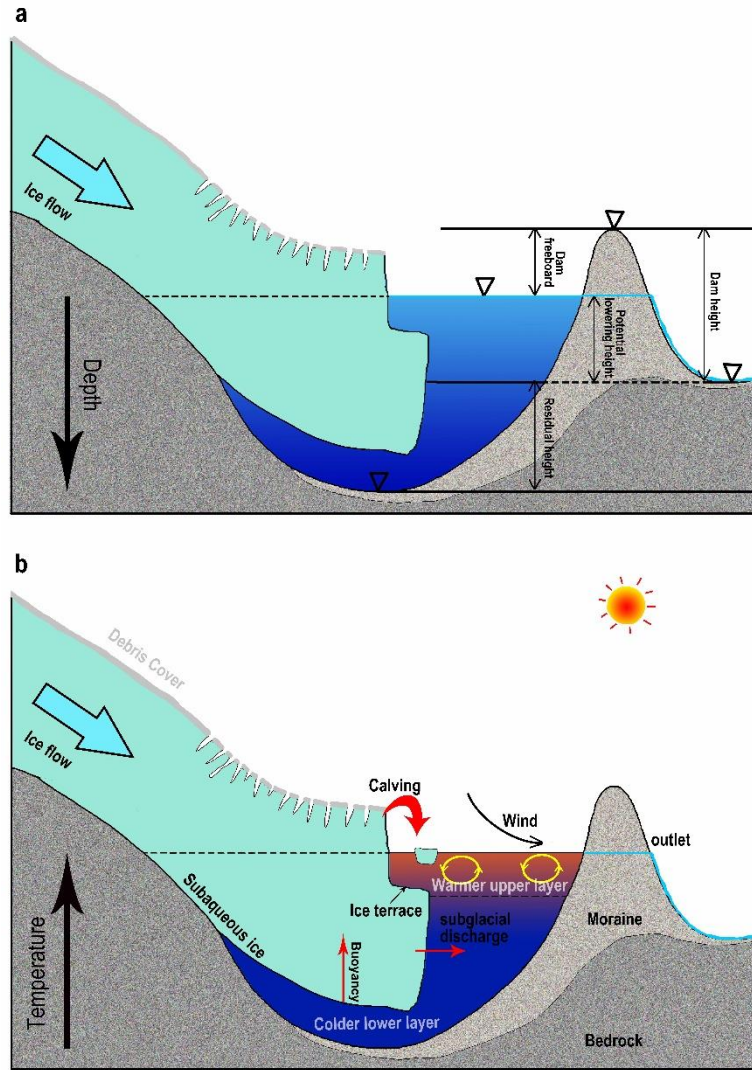
351 ~~(3) Third, the~~ ~~the~~ deepest sites of ~~supraproglacial, periglacial, and extraglacial~~ lakes have been considered to be
352 ~~in the lake center and~~ near the glacier-lake interface ~~for proglacial lakes and ice dammed lakes~~. The developing
353 proglacial lakes, however, are complex. Their deepest sites are constantly located near the glacier terminus before
354 the deepest site of overdeepening is exposed (Fig. 9a), which is in accordance with our hypothesis. With the deepest
355 sites developing more fully, they gradually shift toward the lake center. Our algorithm has not addressed these
356 changes. ~~–~~ In the future, the conceptual model ~~will require~~ ~~–~~ ~~parameter optimization~~ ~~optimization through~~
357 learning with a number of measured bathymetry data. Furthermore, the present version of our algorithm relies on
358 simple programming and semi-automated geospatial analysis tools processing. We will further develop this
359 conceptual model to create an interface that can automatically process and ~~lessen~~ ~~reduce~~ subjective errors.

360 4.3 Rationality of empirical V-A equations

361 ~~Currently, many studies have attempted to fit V-A equations with regional or~~ ~~claimed~~ ~~global applicability for~~
362 ~~various types of glacial lakes (Cook et al., 2015; Qi et al., 2022). The most common classification method for glacial~~
363 ~~lakes is based on dam materials, such as moraine-dammed, bedrock-dammed, and landslide-dammed. However, this~~
364 ~~study reveals that the different types of glacial lakes have different ideal basin shapes that may be unfavorable to~~
365 ~~most already formed V-A empirical formulations, although some have high R² values (Table 1). For instance, most~~
366 ~~of the proglacial and periglacial lakes is generally dammed by moraine, involving in many fitting works of V-A~~

367 relationships. Unreasonably, the incompletely developed basins of proglacial lakes and the fully developed basins of
368 periglacial lakes are often described by same empirical formulas (Fig. 9a), disregarding the distinct basin
369 development stages between them. This aspect has overlooked in the previous studies. In our fitted curves of V-A
370 relationships for various types of glacial lakes (Fig. 4), the V-A relationship for proglacial lakes is robust, indicating
371 possible global applicability. However, the V-A relationships for periglacial and extraglacial lakes exhibit many
372 outliers, suggesting a stronger influence from exogenous materials ~~for~~filling in these lakes based on our hypothesis.
373 The V-A relationships of these glacial lakes decoupled with their glaciers at least require parameters related to the
374 glacier characteristics and time of detachment for further description.

375 There is no single classification method can adequately capture the refined characteristics of glacial lakes. Even
376 lakes classified as the same type may differ in terms of parent glaciers, bedrock properties, or dam materials. In the
377 modeling of glacial lake bathymetric distribution, accurately estimating the total volume and maximum water depth
378 of glacial lakes is crucial. Therefore, future studies should not only focus on whether the empirical formula is
379 generalizability or global applicability, but also develop more detailed classification criteria for glacial lakes,
380 comprehensively considering dam materials, topological positions, glacier properties, area intervals, geographic
381 location, and other relevant factors. This will facilitate a well-fitting of regional empirical relationships of V-A and
382 D-A for various types of glacial lakes, thereby reducing the dispersion between data points.



384

385 **Figure 9.** The schematic diagrams illustrate (a) the potential maximum lowering height of the glacial lake water level after drainage and
 386 (b) the interactions between the parent glacier and its terminating lake.

387 **4.4 Applications in GLOF modeling**

388 The applicability of a glacial lake bathymetric distribution has been addressed in this study; one such application
 389 is in GLOF modeling. The results make two significant contributions to future GLOF modeling: (i) accurately
 390 estimate the maximum potential outburst water volume of a glacial lake by combining lake surface elevation, dam
 391 bottom elevation, and the optimal GCM; (ii) facilitate coupling between the various GLOF processes in modeling
 392 (trigger—displacement wave—dam breach—flood propagation). Many recent studies have documented
 393 reconstructing the historical GLOFs and simulating the future GLOFs from high outburst potential glacial lakes
 394 (Allen et al., 2015; Anaconda et al., 2015b; Erokhin et al., 2017; Kougkoulos et al., 2018). The modeling precision is

395 expected to improve significantly.

396 On the one hand, most prior studies replaced the potential maximum outburst volume with the total water volume
397 because of the limitations of glacial lake bathymetric investigations (Zhang et al., 2021). Although this could present
398 a maximized risk assessment, an inflated downstream exposure might raise excessive concerns among the authorities
399 and the public regarding inadequate prevention and mitigation measures (Emmer et al., 2022b). As long as the dam's
400 lowest elevation exceeds that of the glacial lake (potential lowering height is less than the maximum water depth), it
401 could result in incomplete drainage (Fig. 8a9a).

402 On the other hand, due to the complicated phase transition in the chain process of GLOFs, a segmented
403 simulation has been generally conducted. For instance, Rapid Mass Movement Simulation (RAMMS) can be used to
404 simulate the impact of ice avalanches or landslides on glacial lakes (Frey et al. 2018; Sattar et al. 2021), and
405 hydrological algorithms are used to calculate the displacement wave (Heller et al. 2009; Evers et al. 2019). Modeling
406 software like IBER, HEC-RAS, or FLO-2D are employed to simulate downstream flood propagation (Alho and
407 Aaltonen, 2008; Osti and Egashira, 2009; Schneider et al., 2014; Somos-Valenzuela et al., 2015; Maurer et al., 2020;
408 Nie et al. 2020).

409 In contrast to a holistic simulation, such a segmented simulation approach undoubtedly causes poor articulation
410 and increased uncertainty in different processes. With the recent scientific developments, a newly developed three-
411 phase flow model, r.avaflow (Mergili et al., 2017), started to be used to simulate GLOF propagations (Mergili et al.,
412 2018, 2020) and can realize the whole hazard cascade modeling with a high performance (Zheng et al., 2021). Our
413 study can provide much-needed glacial lake bathymetry data for such modeling to calculate the displacement wave
414 in the lake surface and the water release process during dam erosion.

415 **4.4–5 Potential developments of numerical or physical models**

416 The standardized glacial lake basin can facilitate other future model development related to glacial lakes and
417 improve knowledge of how the proglacial lakes and lake-terminating glaciers interact. Carrivick et al. (2020)
418 discussed six major challenges in constructing a numerical model of interactions between proglacial lakes and
419 glaciers, which include the imperative for glacial lake bathymetry. The standardized shape implicates the design of
420 the model's basic architecture.

421 Compared with the somewhat realistic glacier bed topography within the overdeepenings revealed by Ice

422 Thickness Models, a standardized lake basin provides an alternative scheme. For a specific proglacial lake, its water
423 level, water temperature, in/outflow, internal circulation, and interface with the glacier vary with glacier-lake
424 dynamics and time, which are very complex processes (Sugiyama et al., 2016; Sutherland et al., 2020). Deep and
425 large proglacial lakes are prone to water stratification due to warmer upper layers and colder lower layers of water
426 because these freshwater terminating lakes currently have no evidence of active internal circulation (Haresign and
427 Warren, 2005; Boyce et al., 2007). This stratification induces the subaqueous ice differential melting and ice terrace
428 formation (Fig. ~~8b~~9b), impacting the glacier terminal calving regimes (Sugiyama et al., 2019; Mallalieu et al., 2020).

429 On the other hand, the dynamic characteristics of glacier snout, such as bed friction, longitudinal stress, and ice
430 flow velocity, vary distinctively due to the presence of terminating lakes (Sugiyama et al., 2011; Liu et al., 2020).
431 The knowledge and understanding of glacial lakes formation and evolution changes continually. The ultimate goal is
432 to present these processes via computer numerical simulations. Yet, the idealized lake basin can facilitate calculating
433 the mass and energy transport at the interface.

434

435 **5 Conclusion**

436 This study was conducted in response to a circumstance that field investigation was the only approach to obtain
437 glacial lake bathymetry. The relationships of volume–area and maximum water depth–area of glacial lakes were
438 reanalyzed via an inventory of the global glacial lake bathymetry data we compiled. The obtained curves were
439 matched with a power-law relationship. Thus, the types of hemispheres or cones were determined as the conceptual
440 models (idealized geometric shapes) of glacial lakes. The standard lake surface was assumed to be an ellipse.

441 ~~Ten–Nine~~ standard conceptual models were identified. The SCMs for the supraglacial, periglacial, and
442 extraglacial lakes are the hemisphere structured by the elliptical side; the hemisphere structured by the upward-
443 opening parabolic side; the cone structured by the straight side; and the cone structured by the rightward-opening
444 parabolic side. The SCMs for the proglacial lakes were determined to be half of the aforementioned four SCMs. Two
445 SCMs were considered for the ice-dammed lakes: the semi–cone structured by the straight side and the triangular
446 cone. To depict the volume between the two SCMs, a general conceptual model was defined ~~that to~~ represents the
447 transition from one SCM to another.

448 Several hypotheses are important in our algorithm to nest the actual glacial lake shapes from idealized

449 conceptual models and interpolate glacial lake bathymetric distribution. First, the supraglacial, periglacial, and
450 extraglacial lakes' deepest sites were assumed to be in the lake center, whereas the proglacial lakes and ice-dammed
451 lakes' deepest sites were near the glacier-lake interface. Second, the effects of exogenous materials and boundary
452 conditions were used to explain the different rates of inward deepening of glacial lakes. ~~Three-Six~~ glacial lakes with
453 measured bathymetry data were selected in the ~~Himalaya region~~ ~~High Mountain Asia~~ ~~Third Pole region~~ for comparison
454 with the simulated bathymetric distributions. The results demonstrated good accuracy and applicability of our
455 conceptual models in estimating lake bathymetry. Relatively high consistency was shown in the point-to-point
456 comparisons of the measured and simulated water depths. _

457 This study constructed the glacial lake bathymetric distribution model ~~in first~~ which is very rewarding for
458 comprehending the evolution of glacial lakes. Moreover, the quality of GLOF modeling and risk assessment is also
459 enhanced by our outlined general conceptual model. These standardized lake basins implicate the design of the
460 model's basic architecture, which can potentially promote the development of future numerical or physical models
461 of glacial lakes.

462

463 *Code availability.* The codes for calculating the functional equations of a general conceptual model in the coordinate
464 axes are available on request.

465 *Data availability.* The observed bathymetric data of Jialongco and Longbasaba Lake were provided by Dr. Xiaojun
466 Yao and [Donghui](#) Shangguan ~~Donghui~~, respectively. The observed bathymetric data of Poiqu NO.1, Dasuopuco, and
467 Maqiongco can be feely downloaded at <https://doi.org/10.6084/m9.figshare.21569175> (Zhang et al., 2023).

468 *Supplement.* The supplement related to this article is available online at: [https://tc.copernicus.org/preprints/tc-2023-](https://tc.copernicus.org/preprints/tc-2023-12/tc-2023-12-supplement.zip)
469 [12/tc-2023-12-supplement.zip](https://tc.copernicus.org/preprints/tc-2023-12/tc-2023-12-supplement.zip).

470 *Author contributions.* TZ and WW designed the study, compiled the data and drafted the manuscript. ~~WW and~~ BA
471 revised and edited the manuscript.

472 *Competing interests.* The authors declare that they have no conflict of interest.

473 *Acknowledgements.* We thank the two anonymous reviewers, Dr. Adam Emmer and the editor, Xichen Li, for the
474 constructive comments that improved the paper.

475 *Financial support.* This study was supported by the Second Tibetan Plateau Scientific Expedition and Research
476 (STEP) Program (2019QZKK0208); the Strategic Priority Research Program of the Chinese Academy of Sciences
477 (XDA20100300); and the International Partnership Program of Chinese Academy of Sciences
478 (131C11KYSB20200029).

479

480 **References**

- 481 Aggarwal, S., Rai, S. C., Thakur, P. K., and Emmer, A.: Inventory and recently increasing GLOF susceptibility of glacial lakes in Sikkim,
482 Eastern Himalaya, *Geomorphology*, 295, 39–54, <http://dx.doi.org/10.1016/j.geomorph.2017.06.014>, 2017.
- 483 Alho, P., and Aaltonen, J.: Comparing a 1D hydraulic model with a 2D hydraulic model for the simulation of extreme glacial outburst
484 floods, *Hydrol. Process*, 22, 1537–1547. <http://dx.doi.org/10.1002/hyp.6692>, 2018.
- 485 Allen, S. K., Rastner, P., Arora, M., Huggel, C., and Stoffel, M. (2016). Lake outburst and debris flow disaster at Kedarnath, June 2013:
486 hydrometeorological triggering and topographic predisposition, *Landslides*, 13, 1479–1491, [http://dx.doi.org/10.1007/s10346-015-](http://dx.doi.org/10.1007/s10346-015-0584-3)
487 0584-3, 2015.
- 488 Anaconda, P. I., Mackintosh, A., Norton, K. P.: Hazardous processes and events from glacier and permafrost areas: lessons from the
489 Chilean and Argentinean Andes, *Earth Surf. Process Landf.*, 40, 2–21, <http://dx.doi.org/10.1002/esp.3524>, 2015a.
- 490 Anaconda, P. I., Mackintosh, A., Norton, K.: Reconstruction of a glacial lake outburst flood (GLOF) in the Engano Valley, Chilean
491 Patagonia: Lessons for GLOF risk management, *Sci. Total Environ.*, 527–528, 1–11,
492 <http://dx.doi.org/10.1016/j.scitotenv.2015.04.096>, 2015b.
- 493 Bolch, T., Buchroithner, M. F., Peters, J., Pradhan, B., Buchroithner, M., and Blagoveshchensky, V.: Identification of glacier motion and
494 potentially dangerous glacial lakes in the mt. Everest region/Nepal using spaceborne imagery, *Nat. Hazard Earth Syst.*, 8, 1329–
495 1340, <http://dx.doi.org/10.1007/s11069-011-9860-2>, 2011.
- 496 Boyce, E. S., Motyka, R. J., and Truffer, M.: Flotation and retreat of a lake-calving terminus, Mendenhall Glacier, southeast Alaska,
497 USA, *J. of Glaciol.*, 53, 211–224, <http://dx.doi.org/10.3189/172756507782202928>, 2007.
- 498 Carrivick, J. L., and Tweed, F. S.: Proglacial lakes: character, behaviour and geological importance, *Quat. Sci. Rev.*, 78, 34–52,
499 <http://dx.doi.org/10.1016/j.quascirev.2013.07.028>, 2013.
- 500 Carrivick, J. L., and Tweed, F. S.: A global assessment of the societal impacts of glacier outburst floods, *Glob. Planet. Change*, 144, 1–
501 16, <http://dx.doi.org/10.1016/j.gloplacha.2016.07.001>, 2016.
- 502 Carrivick, J. L., Tweed, F. S., Sutherland, J. L., and Mallalieu, J.: Toward numerical modeling of interactions between ice-marginal
503 proglacial lakes and glaciers, *Front. Earth Sci.*, 500, <https://doi.org/10.3389/feart.2020.577068>, 2020.
- 504 [Chen, N. S., Hu, G. S., Deng, W., Khanal, N., Zhu, Y. H., and Han, D.: On the water hazards in the trans-boundary Kosi River basin,](#)
505 [Nat. Hazard Earth Syst. Sci., 13, 795–808, http://dx.doi.org/10.1007/978-981-10-2890-8_17, 2013.](#)
- 506 Cook, S. J., Quincey, D. J.: Estimating the volume of Alpine glacial lakes, *Earth Surf. Dyn.*, 3, 559–575, [http://www.earth-surf-](http://www.earth-surf-dynam.net/3/559/2015/doi:10.5194/esurf-3-559-2015)
507 [dynam.net/3/559/2015/doi:10.5194/esurf-3-559-2015](http://www.earth-surf-dynam.net/3/559/2015/doi:10.5194/esurf-3-559-2015), 2015.
- 508 [Coulombe, S., Fortier, D., Bouchard, F., Paquette, M., Charbonneau, S., Lacelle, D., Laurion, I. and Pienitz, R. Contrasted](#)
509 [geomorphological and limnological properties of thermokarst lakes formed in buried glacier ice and ice-wedge polygon terrain,](#)
510 [Cryosphere, 16, 2837–2857. https://doi.org/10.5194/tc-16-2837-2022, 2022.](#)
- 511 Drenkhan, F., Huggel, C., Guardamino, L., and Haeblerli, W.: Managing risks and future options from new lakes in the deglaciating
512 Andes of Peru: The example of the Vilcanota-Urubamba basin, *Sci. Total Environ.*, 665, 465–483,
513 <https://doi.org/10.1016/j.scitotenv.2019.02.070>, 2019.
- 514 Echelmeyer, K., Wang Z. X.: Direct observation of basal sliding and deformation of basal drift at sub-freezing temperatures, *J. Glaciol.*,

515 33, 83–98. <http://dx.doi.org/10.3189/s0022143000005396>, 1987.

516 Emmer, A., and Vilímek, V.: New method for assessing the susceptibility of glacial lakes to outburst floods in the Cordillera Blanca,
517 Peru, *Hydrol. Earth Syst. Sci.*, 18, 3461–3479, <http://www.hydrol-earth-syst-sci.net/18/3461/2014/doi:10.5194/hess-18-3461-2014>,
518 2014.

519 Emmer, A., Klimeš, J., Mergili, M., Vilímek, V. and Cochachin, A.: 882 lakes of the Cordillera Blanca: An inventory, classification,
520 evolution and assessment of susceptibility to outburst floods, *Catena*, 147, 269–279, <http://dx.doi.org/10.1016/j.catena.2016.07.032>,
521 2016.

522 [Emmer, A., Allen, S.K., Carey, M., Frey, H., Huggel, C., Korup, O., Mergili, M., Sattar, A., Veh, G., Chen, T.Y., Cook, S.J., Correas-](#)
523 [Gonzalez, M., Das, S., Diaz Moreno, A., Drenkhan, F., Fischer, M., Immerzeel, W.W., Izagirre, E., Joshi, R.C., Kougkoulos, I.,](#)
524 [Kuyakanon Knapp, R., Li, D., Majeed, U., Matti, S., Moulton, H., Nick, F., Piroton, V., Rashid, I., Reza, M., Ribeiro de Figueiredo,](#)
525 [A., Riveros, C., Shrestha, F., Shrestha, M., Steiner, J., Walker-Crawford, N., Wood, J.L. and Yde, J.C. Progress and challenges in](#)
526 [glacial lake outburst flood research \(2017–2021\): a research community perspective, *Nat. Hazard Earth Sys. Sci.*, 22, 3041–3061.](#)
527 <https://doi.org/10.5194/nhess-22-3041-2022>, 2022a.

528 [Emmer, A., Wood, J.L., Cook, S.J., Harrison, S., Wilson, R., Diaz-Moreno, A., Reynolds, J.M., Torres, J.C., Yarleque, C., Mergili, M.,](#)
529 [Jara, H.W., Bennett, G., Caballero, A., Glasser, N.F., Melgarejo, E., Riveros, C., Shannon, S., Turpo, E., Tinoco, T., Torres, L.,](#)
530 [Garay, D., Villafane, H., Garrido, H., Martinez, C., Apaza, N., Araujo, J. and Poma, C. 160 glacial lake outburst floods \(GLOFs\)](#)
531 [across the Tropical Andes since the Little Ice Age, *Global Plane. Change*, 208. <https://doi.org/10.1016/j.gloplacha.2021.103722>,](#)
532 [2022b.](#)

533 Erokhin, S. A., Zaginaev, V. V., Meleshko, A. A., Ruiz-Villanueva, V., Petrakov, D. A., Chernomorets, S. S., Viskhadzhieva, K. S.,
534 Tutubalina, O. V., and Stoffel, M.: Debris flows triggered from non-stationary glacier lake outbursts: the case of the Teztor Lake
535 complex (Northern Tian Shan, Kyrgyzstan), *Landslides*, 15, 83–98, <http://dx.doi.org/10.1007/s10346-017-0862-3>, 2018.

536 Evans, S. G.: The maximum discharge of outburst floods caused by the breaching of man-made and natural dams, *Can. Geotech. J.*,
537 23(3), 385–387, <http://dx.doi.org/10.1139/t87-062>, 1986.

538 Evers F. M., Heller, V., Fuchs, H., Hager, W. H., and Boes, R. M.: Landslide-generated Impulse Waves in Reservoirs: Basics and
539 Computation, *VAW-Mitteilungen*, 254, 2019.

540 Falatkova, K., Šobr, M., Neureiter, A., Schöner, W., Janský, B., Häusler, H., Engel, Z., and Beneš, V.: Development of proglacial lakes
541 and evaluation of related outburst susceptibility at the Adygin ice-debris complex, northern Tien Shan, *Earth Surf. Dyn.*, 7, 301–
542 320, <https://doi.org/10.5194/esurf-7-301-2019>, 2019.

543 [Field, H.R., Armstrong, W.H. and Huss, M. Gulf of Alaska ice-marginal lake area change over the Landsat record and potential physical](#)
544 [controls, *Cryosphere*, 15, 3255–3278. <https://doi.org/10.5194/tc-15-3255-2021>, 2021.](#)

545 Frey, H., Huggel, C., Chisolm, R. E., Baer, P., McArdeell, B., Cochachin, A., and Portocarrero, C.: Multi-source glacial lake outburst
546 flood hazard assessment and mapping for Huaraz, Cordillera Blanca, Peru, *Front. Earth Sci.*, 6, 210.
547 <https://doi.org/10.3389/feart.2018.00210>, 2018.

548 Fujita, K., Sakai, A., Takenaka, S., Nuimura, T., Surazakov, A. B., Sawagaki, T., and Yamanokuchi, T.: Potential flood volume of
549 Himalayan glacial lakes, *Nat. Hazard Earth Syst. Sci.*, 13, 1827–1839, [http://www.nat-hazards-earth-syst-](http://www.nat-hazards-earth-syst-sci.net/13/1827/2013/doi:10.5194/nhess-13-1827-2013)
550 [sci.net/13/1827/2013/doi:10.5194/nhess-13-1827-2013](#), 2013.

551 Haresign, E., and Warren, C. R.: Melt rates at calving termini: a study at Glaciar León, Chilean Patagonia, Geological Society, London,
552 *Special Publications*, 242, 99–109, <http://dx.doi.org/10.1144/GSL.SP.2005.242.01.09>, 2005.

553 Heller, V., Hager, W. H., Minor, H. E.: *Landslide Generated Impulse Waves in Reservoirs*, Zurich: Mitteilungen Versuchsanstalt für
554 Wasserbau, Hydrologie und Glaziologie (VAW), ETH Zürich, 2019.

555 Huggel, C., Kääh, A., Haeblerli, W., Haeblerli, W., Teyssie, P., and Paul, F.: Remote sensing based assessment of hazards from glacier
556 lake outbursts: a case study in the Swiss Alps, *Can. Geotech. J.*, 39, 316–330, <http://dx.doi.org/10.1139/t01-099>, 2002.

557 Hugonnet, R., McNabb, R., Berthier, E., Menounos, B., Nuth, C., Girod, L., Farinotti, D., Huss, M., Dussailant, I., Brun, F., and Kääh,
558 A.: Accelerated global glacier mass loss in the early twenty-first century, *Nature*, 592, 726–731, <https://doi.org/10.1038/s41586->

559 021-03436-z, 2021.

560 Kapitsa, V., Shahgedanova, M., Machguth, H., Severskiy, I., and Medeu, A.: Assessment of evolution and risks of glacier lake outbursts
561 in the Djungarskiy Alatau, Central Asia, using Landsat imagery and glacier bed topography modelling, *Nat. Hazard Earth Syst. Sci.*,
562 17, 1837–1856, <https://doi.org/10.5194/nhess-17-1837-2017>, 2017.

563 Khanal, N. R., Hu, J. M., and Mool, P.: Glacial lake outburst flood risk in the Poiqu/Bhote Koshi/Sun Koshi river basin in the Central
564 Himalayas, *Mt. Res. Dev.*, 35, 351–364, <http://dx.doi.org/10.1659/MRD-JOURNAL-D-15-00009>, 2015.

565 Kougkoulos, I., Cook, S. J., Edwards, L. A., Clarke, L. J., Symeonakis, E., Dortch, J. M., and Nesbitt, K.: Modelling glacial lake outburst
566 flood impacts in the Bolivian Andes, *Nat. Hazard*, 94, 1415–1438, <https://doi.org/10.1007/s11069-018-3486-6>, 2018.

567 Li, D., Shangguan, D. H., Wang, X., Ding, Y. J., Su, P. C., Liu, R. L., and Wang, M. X.: Expansion and hazard risk assessment of glacial
568 lake Jialong Co in the central Himalayas by using an unmanned surface vessel and remote sensing, *Sci. Total Environ.*, 784,
569 <https://doi.org/10.1016/j.scitotenv.2021.147249>, 2021.

570 Linsbauer, A., Frey, H., Haeblerli, W., Machguth, H., Azam, M. F., and Allen, S.: Modelling glacier-bed overdeepenings and possible
571 future lakes for the glaciers in the Himalaya—Karakoram region, *Ann. Glaciol.*, 57, 119–130,
572 <http://dx.doi.org/10.3189/2016AoG71A627>, 2016.

573 Liu, Q., Mayer, C., Wang, X., Nie, Y., Wu, K. P., Wei, J. F., and Liu, S. Y.: Interannual flow dynamics driven by frontal retreat of a lake-
574 terminating glacier in the Chinese Central Himalaya, *Earth Planet. Sci. Lett.*, 546, 116450,
575 <https://doi.org/10.1016/j.epsl.2020.116450>, 2020.

576 Lliboutry, L., Arnao, B. M., Pautre, A., and Schneider, B.: Glaciological problems set by the control of dangerous lakes in Cordillera
577 Blanca, Peru. I. Historical failures of morainic dams, their causes and prevention, *J. Glaciol.*, 18, 239–254,
578 <http://dx.doi.org/10.1017/S002214300002133X>, 1977.

579 Loriaux, T., Casassa, G.: Evolution of glacial lakes from the Northern Patagonia Icefield and terrestrial water storage in a sea-level rise
580 context, *Glob. Planet. Change*, 102, 33–40, <http://dx.doi.org/10.1016/j.gloplacha.2012.12.012>, 2013.

581 [Lützw, N., Veh, G. and Korup, O. A global database of historic glacier lake outburst floods, *Earth Sys. Sci. Data*, \(in discussion\).
582 <http://dx.doi.org/10.5194/essd-2022-449>, 2023.](https://doi.org/10.5194/essd-2022-449)

583 Ma, J. S., Song, C. Q., Wang, Y. J.: Spatially and Temporally Resolved Monitoring of Glacial Lake Changes in Alps During the Recent
584 Two Decades, *Front. Earth Sci.*, 9, <https://doi.org/10.3389/feart.2021.723386>, 2021.

585 Mallalieu, J., Carrivick, J. L., Quincey, D. J., and Smith, M. W.: Calving seasonality associated with melt-undercutting and lake ice
586 cover, *Geophys. Res. Lett.*, 47, e2019GL086561, <https://doi.org/10.1029/2019GL086561>, 2020.

587 Maurer, J. M., Schaefer, J. M., Russell, J. B., Rupper, S., Wangdi, N., Putnam, A. E., and Young, N.: Seismic observations, numerical
588 modeling, and geomorphic analysis of a glacier lake outburst flood in the Himalayas, *Sci. Adv.*, 6, eaba3645,
589 <http://dx.doi.org/10.1126/sciadv.aba3645>, 2020.

590 Mergili, M., Fischer, J. T., Krenn, J., Pudasaini, S. P.: r. avaflow v1, an advanced open-source computational framework for the
591 propagation and interaction of two-phase mass flows, *Geosci. Model Develop.*, 10, 553–569, <http://dx.doi.org/10.5194/gmd-10-553-2017>, 2017.

592

593 Mergili, M., Emmer, A., Juricova, A., Cochachin, A., Fischer, G. T., Huggel, C., and Pudasaini, S. P.: How well can we simulate complex
594 hydro-geomorphic process chains? The 2012 multi-lake outburst flood in the Santa Cruz Valley (Cordillera Blanca, Peru), *Earth
595 Surf. Process. Landf.*, 431373–1389, <http://dx.doi.org/10.1002/esp.4318>, 2018.

596 Mergili M, Pudasaini SP, Emmer A, Fischer, G. T., Cochachin, A., Frey, H.: Reconstruction of the 1941 GLOF process chain at Lake
597 Palcacocha (Cordillera Blanca, Peru), *Hydrol. Earth Syst. Sci.*, 24, 93–114, <https://doi.org/10.5194/hess-24-93-2020>, 2020.

598 Miles, E. S., Watson, C. S., Brun, F., Berthier, E., Esteves, M., Quincey, D. J., Miles, K. E., Hubbard, B., and Wagnon, P.: Glacial and
599 geomorphic effects of a supraglacial lake drainage and outburst event, Everest region, Nepal Himalaya, *The Cryosphere*, 12, 3891–
600 3905, <https://doi.org/10.5194/tc-12-3891-2018>, 2018.

601 Muñoz, R., Huggel, C., Frey, H., Cochachin, A., and Haeblerli, W.: Glacial lake depth and volume estimation based on a large bathymetric
602 dataset from the Cordillera Blanca, Peru, *Earth Surf. Process. Landf.*, <http://dx.doi.org/10.1002/esp.4826>, 2020.

603 Nie, Y., Liu, Q., Wang, J. D., Zhang, Y. L., Sheng, Y. W., and Liu, S. Y.: An inventory of historical glacial lake outburst floods in the
604 Himalayas based on remote sensing observations and geomorphological analysis, *Geomorphology*, 308, 91–106,
605 <https://doi.org/10.1016/j.geomorph.2018.02.002>, 2018.

606 Nie, Y., Liu, W., Liu, Q., Hu, X., and Westoby, M. J.: Reconstructing the Chongbaxia Tsho glacial lake outburst flood in the Eastern
607 Himalaya: Evolution, process and impacts, *Geomorphology*, 370, 107393, <https://doi.org/10.1016/j.geomorph.2020.107393>, 2020.

608 O'Connor, J. E., Hardison III, J. H., Costa, J. E.: Debris Flows from Failures of Neoglacial-Age Moraine Dams in the Three Sisters and
609 Mount Jefferson Wilderness Areas, Oregon, 105 pp, 2001.

610 Osti, R., and Egashira, S.: Hydrodynamic characteristics of the Tam Pokhari glacial lake outburst flood in the Mt. Everest region, Nepal,
611 *Hydrol. Process.*, 23, 2943–2955, <http://dx.doi.org/10.1002/hyp.7405>, 2009.

612 Patel, L. K., Sharma, P., Laluraj, C. M., Thamban, M., Singh, A., and Ravindra, R.: A geospatial analysis of Samudra Tapu and Gepang
613 Gath glacial lakes in the Chandra Basin, Western Himalaya, *Nat. Hazard*, 86, 1275–1290,
614 <https://link.springer.com/article/10.1007/s11069-017-2743-4>, 2017.

615 Petrov, M. A., Sabitov, T. Y., Tomashevskaya, I. G., Glazirin, G. E., Chernomorets, S. S., Savernyuk, E. A., Tutubalina, O. V., Petrakov,
616 D. A., Sokolov, L. S., Dokukin, M. D., Mountrakis, G., Ruiz-Villanueva, V., and Stoffel, M.: Glacial lake inventory and lake outburst
617 potential in Uzbekistan, *Sci. Total Environ.*, 592, 228–242, <http://dx.doi.org/10.1016/j.scitotenv.2017.03.068>, 2017.

618 [Qi, M. M., Liu, S. Y., Wu, K. P., Zhu, Y., Xie, F. M., Jin, H., Gao, Y. P. and Yao, X. J. Improving the accuracy of glacial lake volume
619 estimation: A case study in the Poiqu basin, central Himalayas, *J. Hydrol.*, 610. <https://doi.org/10.1016/j.jhydrol.2022.127973>, 2022.](https://doi.org/10.1016/j.jhydrol.2022.127973)

620 [Rick, B., McGrath, D., Armstrong, W. and McCoy, S.W. Dam type and lake location characterize ice-marginal lake area change in Alaska
621 and NW Canada between 1984 and 2019, *Cryosphere*, 16, 297–314. <https://doi.org/10.5194/tc-16-297-2022>, 2022.](https://doi.org/10.5194/tc-16-297-2022)

622 Richardson, S. D., Reynolds, J. M.: An overview of glacial hazards in the Himalayas, *Quat. Int.*, 65–6, 31–47,
623 [http://dx.doi.org/10.1016/S1040-6182\(99\)00035-X](http://dx.doi.org/10.1016/S1040-6182(99)00035-X), 2000.

624 Sakai, A.: Glacial lakes in the Himalayas: a review on formation and expansion processes, *Glob. Environ. Res.*, 16, 23–30, 2012.

625 Sattar, A., Haritashya, U. K., Kargel, J. S., Leonard, G. J., Shugar, D. H., and Chase, D. V.: Modeling lake outburst and downstream
626 hazard assessment of the Lower Barun Glacial Lake, Nepal Himalaya, *J. Hydrol.*, 598, 126208,
627 <https://doi.org/10.1016/j.jhydrol.2021.126208>, 2021.

628 Schneider, D., Huggel, C., Cochachin, A., Guillén, S., and García, J.: Mapping hazards from glacier lake outburst floods based on
629 modelling of process cascades at Lake 513, Carhuaz, Peru, *Adv. Geosci.*, 35, 145–155, [http://dx.doi.org/10.5194/adgeo-35-145-](http://dx.doi.org/10.5194/adgeo-35-145-2014)
630 2014, 2014.

631 Sharma, R. K., Pradhan, P., Sharma, N. P., and Shrestha, D. G.: Remote sensing and in situ-based assessment of rapidly growing South
632 Lhonak glacial lake in eastern Himalaya, India, *Nat. Hazard*, 93, 393–409, <https://doi.org/10.1007/s11069-018-3305-0>, 2018.

633 Shugar, D. H., Burr, A., Haritashya, U. K., Kargel, J. S., Watson, C. S., Kennedy, M. C., Bevington, A. R., Betts, R. A., Harrison, S., and
634 Strattman, K.: Rapid worldwide growth of glacial lakes since 1990, *Nat. Clim. Change*, 10, 939–945,
635 <https://doi.org/10.1038/s41558-020-0855-4>, 2020.

636 Somos-Valenzuela, M. A., McKinney, D. C., Byers, A. C., Rounce, D. R., Portocarrero, C., and Lamsal, D.: Assessing downstream flood
637 impacts due to a potential GLOF from Imja Tsho in Nepal, *Hydrol. Earth Syst. Sci.*, 19, 1401–1412, [http://dx.doi.org/10.5194/hess-](http://dx.doi.org/10.5194/hess-19-1401-2015)
638 19-1401-2015, 2015.

639 Sugiyama, S., Skvarca, P., Naito, N., Enomoto, H., Tsutaki, S., Tone, K., Marinsek, S., and Aniya, M.: Ice speed of a calving glacier
640 modulated by small fluctuations in basal water pressure, *Nat. Geosci.*, 4, 597–600, <http://dx.doi.org/10.1038/ngeo1218>, 2011.

641 Sugiyama, S., Minowa, M., Sakakibara, D., Skvarca, P., Sawagaki, T., Ohashi, Y., Naito, N., and Chikita, K.: Thermal structure of
642 proglacial lakes in Patagonia, *J. Geophys. Res.: Earth Surf.*, 121, 2270–2286, <http://dx.doi.org/10.1002/2016JF004084>, 2016.

643 Sugiyama, S., Minowa, M., and Schaefer, M.: Underwater ice terrace observed at the front of Glaciar Grey, a freshwater calving glacier
644 in Patagonia, *Geophys. Res. Lett.*, 46, 2602–2609, <http://dx.doi.org/10.1029/2018GL081441>, 2019.

645 Sugiyama, S., Minowa, M., Fukamachi, Y., Hata, S., Yamamoto, Y., Sauter, T., Schneider, C., and Schaefer, M.: Subglacial discharge
646 controls seasonal variations in the thermal structure of a glacial lake in Patagonia, *Nat. Commun.*, 12, 1–9,

647 <https://doi.org/10.1038/s41467-021-26578-0>, 2021.

648 Sutherland, J. L., Carrivick, J. L., Gandy, N., Shulmeister, J., Quincey, D. J., and Cornford, S. L.: Proglacial lakes control glacier
649 geometry and behavior during recession, *Geophys. Res. Lett.*, 47, e2020GL088865, <https://doi.org/10.1029/2020GL088865>, 2020.

650 Veh, G., Korup, O., and Walz, A.: Hazard from Himalayan glacier lake outburst floods, *PNAS*, 117, 907–912,
651 <https://www.pnas.org/cgi/doi/10.1073/pnas.1914898117>, 2020.

652 Wang, X., Liu, S. Y., Ding, Y. J., Guo, W. Q., Jiang, Z. L., Lin, J., and Han, Y.: An approach for estimating the breach probabilities of
653 moraine-dammed lakes in the Chinese Himalayas using remote-sensing data, *Nat. Hazard Earth Syst. Sci.*, 12, 3109–3122,
654 <http://dx.doi.org/10.5194/nhess-12-3109-2012>, 2012.

655 Wang, X., Guo, X. Y., Yang C. D., Liu, Q. H., Wei, J. F., Zhang, Y., Liu, S. Y., Zhang, Y. L., Jiang, Z. L., and Tang, Z. G.: Glacial lake
656 inventory of high-mountain Asia in 1990 and 2018 derived from Landsat images, *Earth Syst. Sci. Data*, 12, 2169–2182,
657 <https://doi.org/10.5194/essd-12-2169-2020>, 2020.

658 Wang, W. C., Gao, Y., Anacona, P. I., Lei, Y. B., Xiang, Y., Zhang, G. Q., Li, S. H., and Lu, A. X.: Integrated hazard assessment of
659 Cirenmaco glacial lake in Zhangzangbo valley, Central Himalayas, *Geomorphology*, 306, 292–305,
660 <http://dx.doi.org/10.1016/j.geomorph.2015.08.013>, 2018.

661 Watson, C. S., Quincey, D. J., Carrivick, J. L., Smith, M. W., Rowan, A. V., and Richardson, R.: Heterogeneous water storage and thermal
662 regime of supraglacial ponds on debris-covered glaciers, *Earth Surf. Process. Landf.*, 43, 229–241,
663 <http://dx.doi.org/10.1002/esp.4236>, 2018.

664 [Watson, C. S., Kargel, J. S., Shugar, D. H., Haritashya, U. K., Schiassi, E., and Furfaro, R. Mass Loss From Calving in Himalayan
665 Proglacial Lakes Front. Earth Sci. 7, 342. <http://dx.doi.org/10.3389/feart.2019.00342>. 2020.](https://doi.org/10.3389/feart.2019.00342)

666 [Wei, J. F., Liu, S. Y., Wang, X., Zhang, Y., Jiang, Z. L., Wu, K. P., Zhang, Z., and Zhang, T.: Longbasaba Glacier recession and contribution
667 to its proglacial lake volume between 1988 and 2018, *J. Glaciol.*, 67, 473–484, <https://doi.org/10.1017/jog.2020.119>, 2021.](https://doi.org/10.1017/jog.2020.119)

668 Westoby, M. J., Glasser, N. F., Brasington, J., Hambrey, M. J., Quincey, D. J., and Reynolds, J. M.: Modelling outburst floods from
669 moraine-dammed glacial lakes, *Earth-Sci. Rev.*, 134, 137–159, <http://dx.doi.org/10.1016/j.earscirev.2014.03.009>, 2014.

670 Wood, J. L., Harrison, S., Wilson, R., Emmer, A., Yarleque, C., Glasser, N. F., Torres, J. C., Caballero, A., Araujo, J., Bennett, G. L.,
671 Diaz-Moreno, A., Garay, D., Jara, H., Poma, C., Reynolds, J. M., Riveros, C. A., Romero, E., Shannon, S., Tinoco, T., Turpo, E.,
672 and Villafane, H.: Contemporary glacial lakes in the Peruvian Andes, *Glob. Planet. Change*, 204, 103574,
673 <https://doi.org/10.1016/j.gloplacha.2021.103574>, 2021.

674 Yao, T. D., Thompson, L., Yang, W., Yu, W. S., Gao, Y., Guo, X. J., Yang, X. X., Duan, K. Q., Zhao, H. B., Xu, B. Q., Pu, J. C., Lu, A.
675 X., Xiang, Y., Kalltel, D. B., and Joswiak, D.: Different glacier status with atmospheric circulations in Tibetan Plateau and
676 surroundings, *Nat. Clim. Change*, 2, 663–667, <http://www.nature.com/doi/10.1038/nclimate1580>, 2012.

677 Yao, T. D., Xue, Y. K., Chen, D. L., Chen, F. H., Thompson, L., Cui, P., Koike, T., K.-M. Lau, W., Lettenmaier, D., Mosbrugger, V.,
678 Zhang, R. H., Xu, B. Q., Dozier, J., Gillespie, T., Gu, Y., Kang, S. C., Piao, S. L., Sugimoto, S., Ueno, K., Wang, L., Wang, W. C.,
679 Zhang, F., Sheng, Y. W., Guo, W. D., Ailikun, Yang, X. X., Ma, Y. M., Shen, S. S. P., Su, Z. B., Chen, F., Liang, S. L., Liu, Y. M.,
680 Singh, V. P., Yang, K., Yang, D. Q., Zhao, X. Q., Qian, Y., Zhang, Y., and Li, Q.: Recent third pole’s rapid warming accompanies
681 cryospheric melt and water cycle intensification and interactions between monsoon and environment: Multidisciplinary approach
682 with observations, modeling, and analysis, *B. Am. Meteorol. Soc.*, 100, 423–444, <https://doi.org/10.1175/BAMS-D-17-0057.1>,
683 2019.

684 Yao, X. J., Liu, S. Y., Sun, M. P., Wei, J. F., and Guo, W. Q.: Volume calculation and analysis of the changes in moraine-dammed lakes
685 in the north Himalaya: a case study of Longbasaba lake, *J. Glaciol.*, 58, 753–760, <http://dx.doi.org/10.3189/2012JoG11J048>, 2012.

686 Yao, X. J., Liu, S. Y., Han, L., Sun, M. P., and Zhao, L. L.: Definition and classification system of glacial lake for inventory and hazards
687 study, *J. Geogr. Sci.*, 28, 193–205, <https://doi.org/10.1007/s11442-018-1467-z>, 2018.

688 Zemp, M., Huss, M., Thibert, E., McNabb, R., Huber, J., Barandun, M., Machguth, H., Nussbaumer, S. U., Gärtner-roer, I., Thomson,
689 L., Paul, F., Maussion, F., Kutuzov, S., and Cogley, J. G.: Global glacier mass changes and their contributions to sea-level rise from
690 1961 to 2016, *Nature*, 568, 382–386, <https://doi.org/10.1038/s41586-019-1071-0>, 2019.

691 Zhang, G. Q., Yao, T. D., Xie, H. J., Wang, W. C., and Yang, Wei.: An inventory of glacial lakes in the Third Pole region and their changes
692 in response to global warming, *Glob. Planet. Change*, 131, 148–157, <http://dx.doi.org/10.1016/j.gloplacha.2015.05.013>, 2015.

693 [Zhang, G. Q., Bolch, T., Yao, T. D., Rounce, D.R., Chen, W. F., Veh, G., King, O., Allen, S.K., Wang, M. and Wang, W. C. Underestimated](#)
694 [mass loss from lake-terminating glaciers in the greater Himalaya, *Nat. Geosci.*, 16, 1–6. \[https://doi.org/10.1038/s41561-023-01150-\]\(https://doi.org/10.1038/s41561-023-01150-1\)](#)
695 [1, 2023.](#)

696 Zhang, T. G., Wang, W. C., Gao, T. G., and An, B. S.: Simulation and Assessment of Future Glacial Lake Outburst Floods in the Poiqu
697 River Basin, Central Himalayas, *Water*, 13, <https://doi.org/10.3390/w13101376>, 2021.

698 Zhang, T. G., Wang, W. C., An, B. S., Gao, T. G., and Yao, T. D.: Ice thickness and morphological analysis reveal the future glacial lake
699 distribution and formation probability in the Tibetan Plateau and its surroundings, *Glob. Planet. Change*, 216, 103923,
700 <https://doi.org/10.1016/j.gloplacha.2022.103923>, 2022.

701 Zheng, G. X., Mergili, M., Emmer, A., Allen, S., Bao, A. M., Guo, H., and Stoffel, M.: The 2020 glacial lake outburst flood at Jinwuco,
702 Tibet: causes, impacts, and implications for hazard and risk assessment, *The Cryosphere*, 15, 3159–3180, [https://doi.org/10.5194/tc-](https://doi.org/10.5194/tc-15-3159-2021)
703 [15-3159-2021](https://doi.org/10.5194/tc-15-3159-2021), 2021.